LRP 411/90 August 1990

Invited and Contributed Papers
presented at the

Joint Varenna-Lausanne International Workshop on "Theory of Fusion Plasmas" Varenna, Italy, August 27-31, 1990

by the
Theory Group

GLOBAL EXTERNAL IDEAL MAGNETOHYDRODYNAMIC INSTABILITIES IN THREE-DIMENSIONAL PLASMAS

W. Anthony Cooper, Guo Y. Fu

Centre de Recherches en Physique des Plasmas
Association Euratom - Confédération Suisse
Ecole Polytechnique Fédérale de Lausanne, Switzerland

Ralf Gruber, Silvio Merazzi
GASOV-EPFL
CH - 1015 Lausanne, Switzerland

Ulrich Schwenn
Max Planck Institut für Plasmaphysik
Garching, F.R.G.

David V. Anderson
NERSC, Livermore USA

Ideal magnetohydrodynamic (MHD) equilibrium and stability computer codes have been essential tools in both the predictive and interpretive fases of magnetic plasma confinement devices. The roles of the ideal MHD stability codes concentrate on the determination of the stable operating windows for a device and the identification of the conditions that maximize the ratio of the plasma pressure to the magnetic field energy density (commonly referred to as the beta parameter, β). Thus, the stability packages ERATO [1] , PEST [2] and the Keldysh code [3] have been applied extensively to two dimensional (2D) axisymmetric equilibria that model existing devices such as JET, TFTR, D-IIID, JT60 and the design phase of next generation devices such as NET and ITER. Stability packages for three dimensional (3D) plasma confinement configurations have only recently become operational, but have been limited to the study of internal mode structures [4,5]. The 3D code,TERPSICHORE has now been generalized to investigate external ideal MHD instabilities by treating the vacuum region surrounding the plasma as a pressureless and shearless pseudoplasma.

Theoretical comparisons of the internal global stability properties of torsatron configurations based on the stellarator expansion method [6] and of Mercier stability between flux conserving equilibria and equilibria with zero net toroidal

plasma current has led to the conclusion that toroidal currents flowing in the plasma are destabilising [7]. However, the problem of the modification of an externally applied rotational transform and the resulting impact on the stability of internal tearing and kink modes has been analysed by Mikhajlov and Shafranov in a cylindrical approximation where helical fields are averaged and the plasma pressure and magnetic field line curvature are neglected [8]. They find that the destabilizing effect of the toroidal current is not universal.

In this paper, we consider the effect of toroidal plasma currents tailored to flow in the outerpart of the enclosed volume on the global external ideal MHD properties of 3D equilibria that model the ATF torsatron in its standard configuration. If the current reduces the externally applied rotational transform, the stability properties are deteriorated, but if the current increases the transform, the stability properties are enhanced.

We have generated 3D equilibria with nested magnetic flux surfaces using the VMEC code [9]. The Fourier amplitudes of R (distance from the major axis) and Z (distance from the horizontal midplane) of the plasma boundary are prescribed and correspond to the standard ATF configuration in which there is no current in the mid-vertical field coils [10]. We also prescribe the pressure profile p(s) and the toroidal current $2\pi J(s)$ enclosed within each flux surface labelled with the variable s which is proportional to the volume enclosed. Specifically, for the pressure profile, we impose that $p'(0)= p(1)=p'(1)= 0$ and $p'(1/2)$ be a minimum to obtain a bell shaped profile of the form

$$p(s) = p(0) (1 -3s^2 +2s^3), \qquad (1)$$

where we vary β with $p(0)$. For the toroidal current profile, we impose that $J(0)= J'(0)= J''(0)= J'(1)= 0$ and $|J'(2/3)|$ be a maximum to obtain a profile of the form

$$2\pi J(s) = 2\pi J(1) (4s^3 -3s^4), \qquad (2)$$

where $2\pi J(1)$ is the total toroidal current enclosed. The normalisation in VMEC is such that the toroidal magnetic flux $2\pi\Phi(1)$ enclosed in the plasma is π. Subject to this normalisation, we have chosen three sequences of equilibria to investigate:

a) cases with $J(1)= 0$ that correspond to zero net toroidal current

b) cases with $2\pi J(1)=0.5$ that unwind the externally applied transform in the vacuum by15% compared with $J(1)= 0$, and

c) cases with $2\pi J(1)= -0.5$ that wind the externally applied transform in the vacuum up further by 13.5% compared with $J(1)= 0$.

In the vacuum state, the ATF equilibrium with $2\pi J(1)= 0.5$ has a magnetic well region that extends to the inner 60% of the enclosed plasma volume. That with $2\pi J(1)= -0.5$ extends to only the inner 25% of the plasma volume. The finite β equilibria show that the Shafranov shift increases (decreases) significantly when $J>0$ ($J<0$) compared with the zero current case. As an example, a magnetic axis shift of 37% of the distance between the magnetic axis position in the vacuum state and the outer midplane location of the plasma boundary occurs at $\beta = 4\%$ for zero current and at 5% for $2\pi J(1)= -0.5$.

The equilibria that are obtained with VMEC are mapped into the Boozer magnetic flux coordinate system [11] to undertake the stability computation. This choice is made because the field lines become straight and the parallel current can be very accurately constructed [12]. A very efficient Fourier technique is employed to map equilibrium quantities into the Boozer frame [5]. A multigrid type approach is employed to determine the spectrum of modes required to reconstruct the equilibrium in Boozer coordinates. An equilibrium is calculated with a coarse radial mesh and a very broad spectrum is selected for the mapping. Then only the dominant modes in the Boozer coordinates (those for which R_{mn} or Z_{mn} exceed 10^{-7}) are retained for refined radial mesh calculations. For the ATF examples presented here, 128 modes sufficed to satisfy the selection criterion and the error in the radial force balance was almost identical to that calculated in the VMEC coordinates.

The linearised ideal MHD equations in variational form can be expressed as

$$\delta W_p + \delta W_v - \omega^2 \delta W_k = 0, \tag{3}$$

where δW_p represents the internal potential energy of the plasma, δW_v represents the magnetic energy in the vacuum region that surrounds the plasma, δW_k represents the kinetic energy and ω^2 corresponds to the eigenvalue of the system. The potential energy can be described as

$$\delta W_p = \frac{1}{2}\int\int\int d^3x \, [\, C^2 + \gamma p \, | \, \nabla \cdot \xi \, |^2 - D \, | \, \xi \cdot \nabla s \, |^2] \tag{4}$$

where ξ represents the perturbed displacement vector, γ is the adiabatic index and

$$C = \nabla \times (\xi \times \mathbf{B}) + \frac{\mathbf{j} \times \nabla s}{|\, \nabla s \,|^2} (\xi \cdot \nabla s) \tag{5}$$

$$D = \frac{2\,(\mathbf{j} \times \nabla s)\cdot(\mathbf{B}\cdot\nabla)\,\nabla s}{|\nabla s|^4}. \qquad (6)$$

In the plasma domain, the radial variable s satisfies $0 \le s \le 1$. The perturbed displacement vector is represented as

$$\xi = \sqrt{g}\,\xi^s \nabla\theta \times \nabla\phi + \eta\,\frac{(\mathbf{B}\times\nabla s)}{B^2} + \left[\frac{J(s)}{\Phi'(s)B^2}\,\eta - \mu\right]\mathbf{B} \qquad (7)$$

where θ and ϕ are the poloidal and toroidal angles of the Boozer coordinate system, $\sqrt{g}$ is the Jacobian and (ξ^s,η , μ) correspond to the three components (radial, binormal, parallel) of the decomposition of the displacement vector. We impose the incompressibility constraint $\nabla\cdot\xi = 0$ to eliminate μ algebraically from the problem. As a result only stability indices rather than physical growth rates are computed, thus a simplified model kinetic energy is invoked. This reduces the size of the stability problem quite considerably as only two of the three components of the perturbation have to be calculated. The vacuum region is devised as a pressureless and currentless pseudoplasma with nested pseudomagnetic flux surfaces with a coordinate system (s_v,θ_v, ϕ_v) that satisfies the conditions $s_v = s = 1$, $\theta_v = \theta$ at the plasma vacuum interface $\phi_v = \phi$. Two important constraints are imposed in the development of the vacuum domain:
1) the geometry varies smoothly accross the plasma-vacuum interface (PVI)
2) the pseudomagnetic flux surfaces remain nested and do not cross the major axis. A conducting wall can be prescribed in two ways:
a) by extrapolation from the PVI such that the radial derivatives of R, Z and the geometric toroidal angle remain constant and
b) by varying smoothly from the shape of the PVI to an arbitrarily shaped wall. To avoid violating the flux surface nestedness constraint, the first method is appropriate to describe a wall that is close to the PVI while the second method is preferable for a wall that is far away. In the work we present here, a circular axisymmetric wall that reaches close to the major axis is prescribed to model a wall at infinity. The ratio of the diameter of the wall to that of the PVI at the $\phi=\phi_v=0$ midplane is 7.4 and $1\le s_v\le 2$. Invoking as gauge condition that the perturbed vector potential **A** has a vanishing component along a pseudomagnetic field vector **T** that satisfies $\nabla\cdot\mathbf{T} = \mathbf{T}\cdot\nabla s_v = 0$ allows us to express the magnetic energy in the vacuum region as

$$\delta W_V = \frac{1}{2} \int\int\int d^3x \, (\nabla \times (\xi_V \times \mathbf{T}))^2 \qquad (8)$$

where we express the displacement vector in the vacuum region as

$$\xi_V = \sqrt{g_V} \frac{\Phi'(s=1)\, X_V}{(d\Phi_V/ds_V)} \nabla\theta_V \times \nabla\phi_V + \frac{(\mathbf{T} \times \nabla s_V)}{T^2} Y_V \qquad (9)$$

The boundary condition at the PVI, $(\xi_V \cdot \nabla s)\, \mathbf{T} = (\xi \cdot \nabla s)$ reduces to $d\Psi_V/d\Phi_V = \Psi'(1)/\Phi'(1)$ which we extend throughout the plasma domain to avoid introducing fictitious resonances in the vacuum region and $X_V(1,\theta_V,\phi_V) = \xi_S(1,\theta_V,\phi_V)$. The poloidal and toroidal pseudomagnetic flux functions are denoted by Ψ_V and Φ_V respectively. The boundary condition at the conducting wall is $X_V = 0$.

We apply a Fourier series decompostion of the perturbation components ξ^s and η given by

$$\xi^s(s,\theta,\phi) = \sum_l s^{-q_l} X_l(s) \sin(m_l\theta - n_l\phi + \Delta) \qquad (10)$$

$$\eta\,(s,\theta,\phi) = \sum_l Y_l(s) \cos(m_l\theta - n_l\phi + \Delta) \qquad (11)$$

where l is an index that labels the mode number pair (m_l, n_l), Δ is a phase factor, and the exponent $q_l = 0$ for equilibria from codes like VMEC which employ flux zoning. For equilibria in which the radial variable is proportional to the radius rather than the volume enclosed $q_l = 1$ for $m_l = 1$. The decomposition of X_V and Y_V is identical to that of ξ^s and η respectively. Because radial derivatives act only on X_l, a finite hybrid element radial discretisation scheme is applied and the energy principle reduces in the weak form to an eigenvalue problem of the form

$$\mathbf{A}x = \lambda \mathbf{B}x \qquad (12)$$

where $x = (X_l, Y_l)$, the eigenvalue is $\lambda = \omega^2$, the matrices A and B are symmetric and have a special block pentadiagonal structure. An inverse vector iteration procedure is used to invert this equation and determine the smallest eigenvalue of the system. By means of an eigenvalue shift, we are able to find all the eigenvalues of the system [5].

In axisymmetric systems, the toroidal mode numbers are all decoupled one from another. In 3D systems with stellarator symmetry and a finite number of field periods, there are families of toroidal modes numbers that are decoupled one from another. In a 12 field period device like the ATF there are 6 such families. These can be described by (m ; LN±k), where $0 \le m \le \infty$ labels the toroidal mode numbers of the instability, L=12 is the number of field periods, $-\infty \le N \le \infty$ labels in general the toroidal modes that describe the equilibrium state and $1 \le k \le 6$ labels each independent family of toroidal modes that describe the instability structure. Thus for example, k=1 corresponds to immediate toroidal sideband structures of the equilibrium state and include the toroidal modes with n= - 1, 1, 11, 13, 23, 25, etc. The proposed WVII-X device with 5 field periods has 2 families. Toroidal mode numbers with n= -1, 1, 4, 6, 9, 11, etc. constitute one while those with n= 2, 3, 7, 8, 12, 13, etc. constitute the other.

In the calculations we present in this paper, we concentrate on the stability properties of ATF equilibria to global low toroidal mode number n instabilities, though we have carried out also some selected calculations for more localized modes. It is not always an easy task to distinguish high-n ballooning modes from high-n modes destabilized by the finite hybrid element scheme [3]. The procedure we have followed, is to first select a single toroidal mode number with a spectrum of poloidal modes to obtain an eigenvalue λ. We then try to follow this branch as we couple in modes with different toroidal mode numbers. For the cases that we have studied, we find that either with single or multiple toroidal mode numbers, that as we vary the number of radial mesh points, the convergence properties of the eigenvalue are quadratic from the unstable side. The convergence curves with multiple toroidal mode numbers are shifted towards the unstable side compared with single toroidal mode number cases. The shift becomes less pronounced as the marginal point is approached. The number of radial intervals in the vacuum is fixed at one quarter the number of radial intervals in the plasma.

The ATF equilibrium with toroidal current $2\pi J(1) = 0.5$ has already at a value of $\beta = 1.4\%$ a noticeably nonmonotonic rotational transform profile $\iota(s)$ with multiple values of $\iota = 1/2$. The transform at the edge is $\iota = 0.87$. This configuration is strongly unstable to an m=1, n=1 external mode coupled together with a noticeable m=2, n=1 component in the interior of the plasma. The standard zero net toroidal current ATF equilibrium at a value of $\beta = 3.35\%$ also has a nonmonotonic $\iota(s)$ profile but the local minimum in ι remains greater than 1/2. The value at the PVI reaches $\iota = 0.98$. The perturbed pressure distribution at the PVI shows the distinct m=1, n=1 structure of the instability in Fig. 1. The n=2 family only becomes unstable to global structures at $\beta = 3.96\%$, when local minimum in the ι-profile drops below 1/2 and modes with n=2, m=4,5,6,7 make significant contributions. The ATF equilibria with $2\pi J(1) = -0.5$ have the $\iota = 1$

surface inside the plasma, but in a region of very high magnetic shear. As a result, the n=1 family remains stable to global structure beyond β=5% as the m=1, n=1 mode becomes very localized due to the effects of high shear. At a value of β = 4.5%, the ι-profile, though still monotonic, becomes very flat with ι>1/2 in the internal part of the plasma. The n=2 family becomes unstable to global structure dominated by the internal m=3, n=2 mode. This type of structure is evident in the perturbed pressure distribution on the PVI shown in Fig. 2. The bulk of the stability calculations that we have performed are summarized in Fig. 3, where we show the converged eigenvalue that we have determined as a function of the volume averaged β for

1) the sequence of ATF equilibria with a finite toroidal current $2\pi J(1)$=0.5 established by the n=1 family of global external modes, where strong instability subsists well below β=1%,

2) the sequence of ATF equilibria with zero net toroidal current established by the n=1 family of global external modes, at about 3.14%, and

3) the sequence of ATF equilibria with finite toroidal plasma current $2\pi J$ (1)=-0.5 established by the n=2 family of principally global internal modes which has a β limit of about 4.25%.

Benchmark studies of fixed boundary internal MHD stability of flux conserving sequences of ATF equilibria with parabolic pressure profiles for low and high toroidal n mode structures have been performed. These equilibria are stable to the n=1 family of modes up to β =6.7%. At this value of β, the coupling between n=2 and n=-2 modes weakly destabilises the n=2 family. The critical β value drops to 4.1% for the n=3 family of modes and to 3% for the n=9 modes. The higher n modes have very distinct ballooning mode structures.

In summary, we have investigated the global ideal MHD stability properties of the fully 3D standard ATF configuration with a bell-shaped pressure profil and a range of toroidal currents that flow in the outer part of the plasma column. The magnitude of the currents were very modest altering the rotational transform by $\pm$ 15% compared with the standard zero current case. Such small tailored currents could easily be produced with an ECRH current drive. Nevertheless, the MHD stability properties of the configuration were modified significantly. The zero current case has a β limit of 3.14% imposed by the n=1 family of modes. If the current imposed unwinds the externally applied transform, the stability properties deteriorate and the configuration is unstable below β =1%. If the current winds the externally applied transform further, the n=1 family is stabilised and the n= 2 family imposes a limit at β= 4.25%.

This work was financed by the Swiss National Science Foundation and Euratom.

References :

[1] R. Gruber, F. Troyon, D. Berger, L.C. Bernard, S. Rousset, R. Schreiber, W. Kerner, W. Schneider, K.V. Roberts, ' ERATO stability code', Comput. Phys. Commun. **21** (1981) 323-371

[2] R.C. Grimm, J.M. Greene, J.L. Johnson, ' Computation of the MHD spectrum in axisymmetric toroidal confinement systems', Meth. Comput. Phys. **16** (1976) 253-280

[3] L.M. Degtyarev, S.Yu. Medvedev, ' Methods for numerical simulation of ideal MHD stability of axisymmetric plasmas ', Comput. Phys. Commun. **43** (1986) 29-56

[4] C. Schwab, in *Proc. of the Joint Varenna-Lausanne International Workshop on Theory of Fusion Plasmas*, (Editrice Compositori, Bologna, 1988) 52

[5] D.V. Anderson, W.A. Cooper, U. Schwenn, R. Gruber, ' Linear MHD stability analysis of toroidal 3-D equilibria with TERPSICHORE', in *Proc. of the Joint Varenna-Lausanne International Workshop on Theory of Fusion Plasmas*, (Editrice Compositori, Bologna, 1988) 93-102

[6] J.M Greene, J.L. Johnson, Phys. Fluids **4** (1961) 875.

[7] N. Dominguez et al., Nucl. Fusion **29** (1989) 2079

[8] M.I. Mikhajlov and V.D. Shafranov, Nucl. Fusion **30** (1990) 413

[9] S.P. Hirshman, U. Schwenn, J. Nührenberg, ' Improved radial differencing for 3D MHD equilibrium calculations', J. Comput. Phys. **87** (1989) 396.

[10] J.F. Lyon et al., Fusion Technology **10** (1986) 179

[11] A.H. Boozer, Phys. Fluids **23** (1980) 804

[12] J. Nührenberg, R. Zille, ' Equilibrium and stability of low-shear stellarators', in *Proc. of Workshop on theory of fusion plasmas* (Editrice Compositori, Bologna, 1987), EUR11336EN, 3-23

Fig. 1. Perturbed pressure distribution of ATF with J=0 -- external n=1 instability

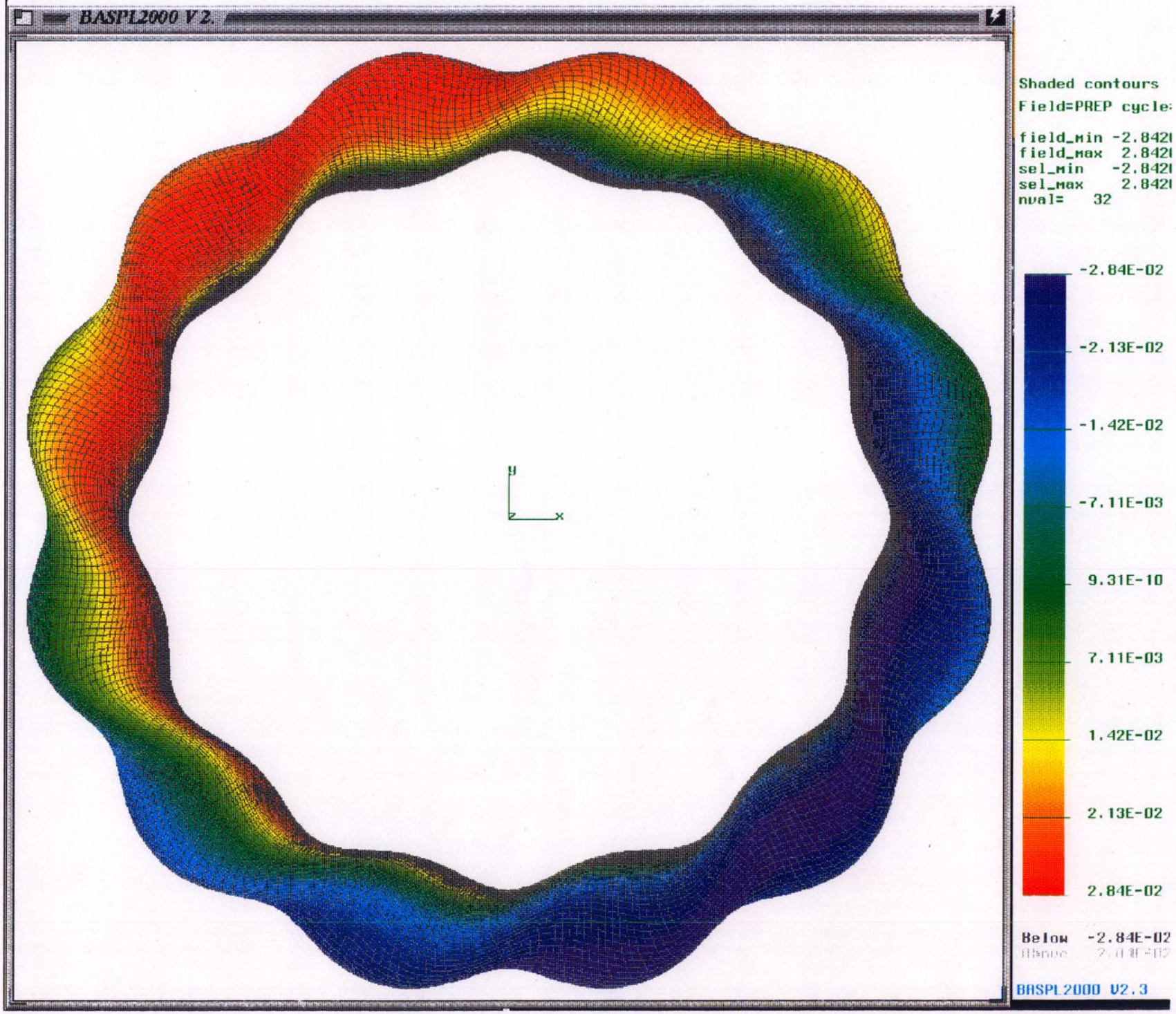

Fig. 2. Perturbed pressure distribution of ATF with J<0 -- internal n=2 instability

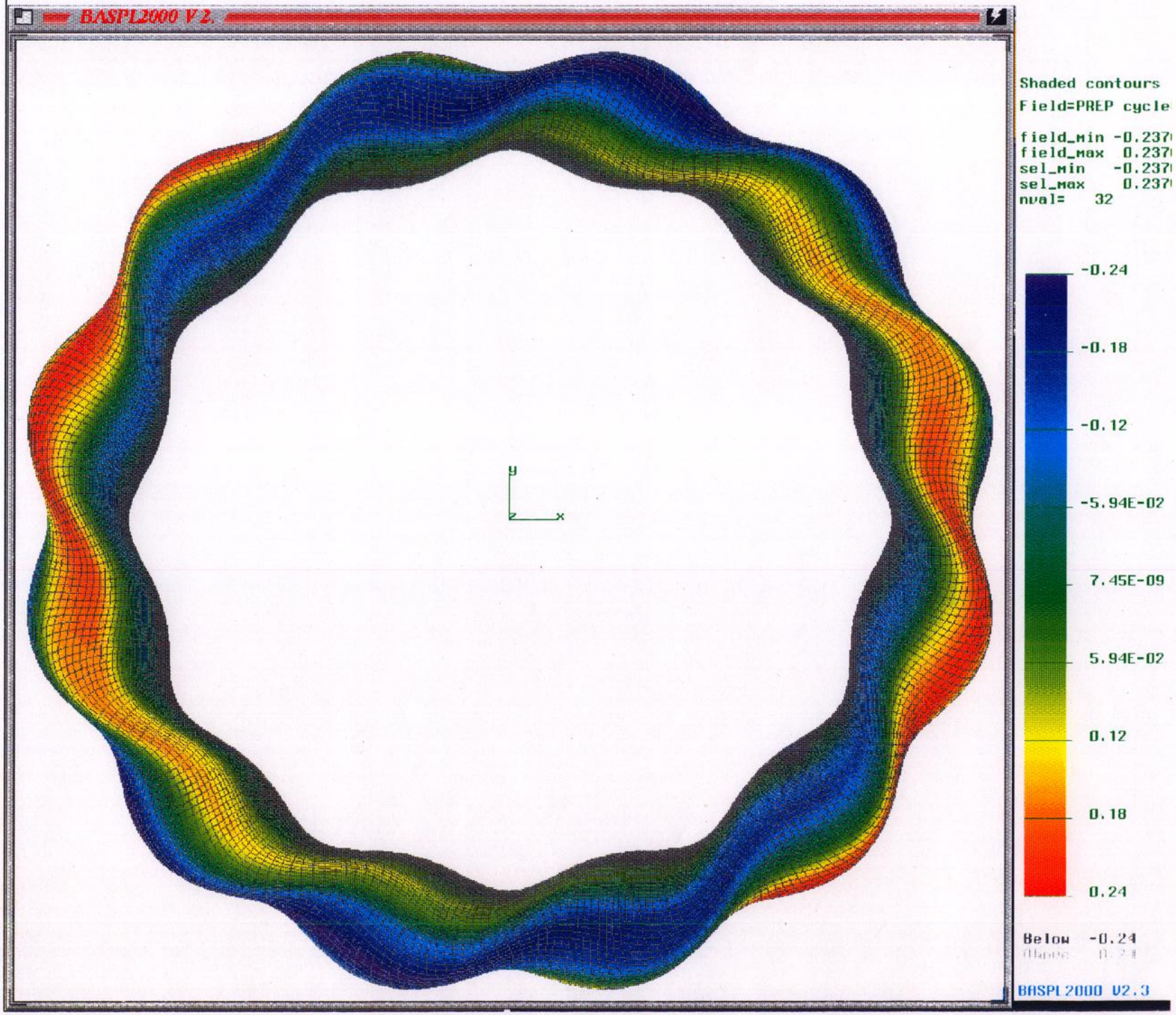

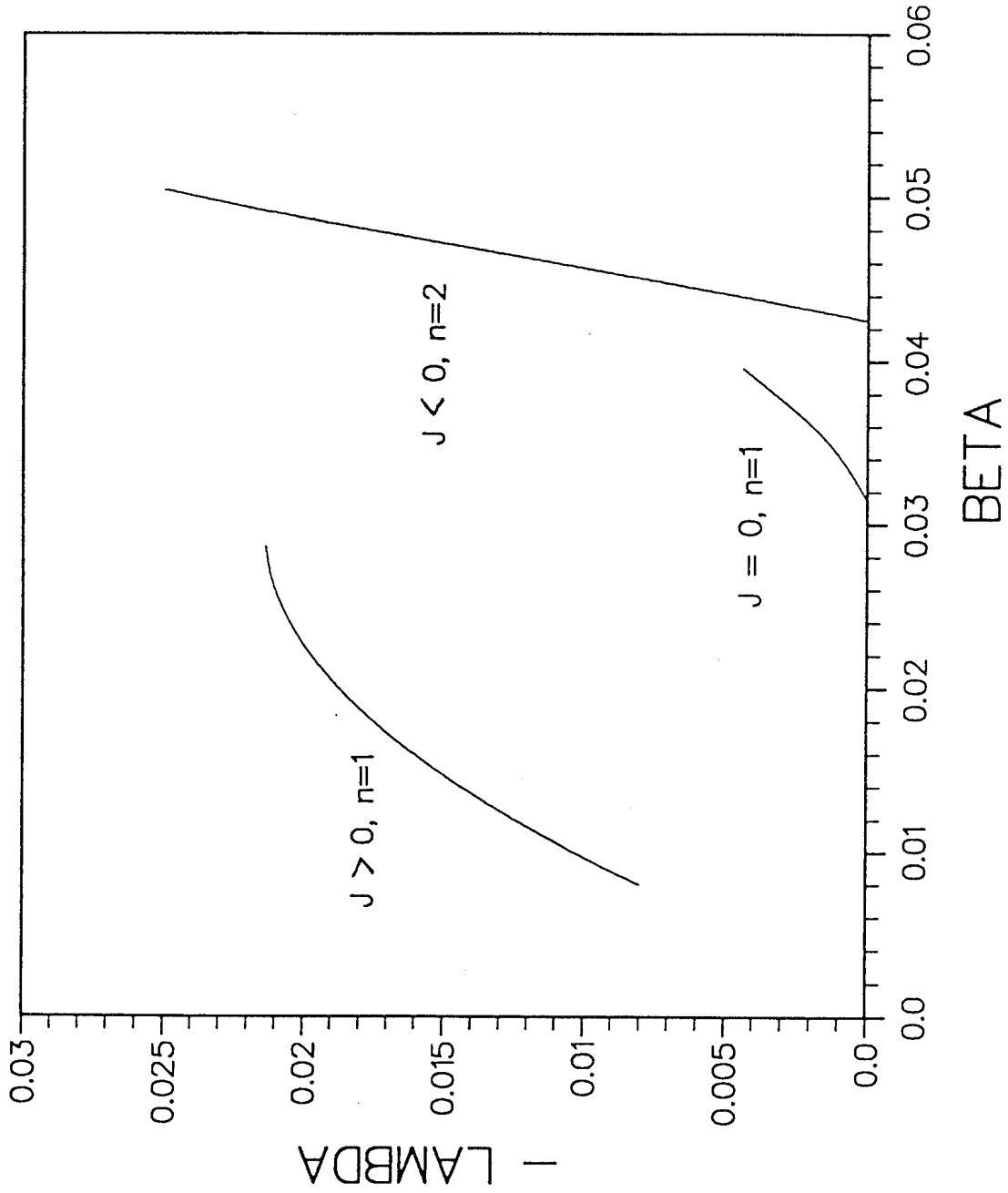

Fig. 3. Converged eigenvalue versus beta

A MODIFIED ELECTROMAGNETIC WAVE EQUATION

X. Llobet, K. Appert, and J. Vaclavik

Centre de Recherches en Physique des Plasmas
Association Euratom - Confédération Suisse
Ecole Polytechnique Fédérale de Lausanne
21, av. des Bains - 1007 Lausanne / Switzerland

The aim of this paper is to find an alternative to the usual electromagnetic wave equation: that is, we want to find a different equation with the same solutions. The final goal is to solve electromagnetic problems with iterative methods. The **curl curl** operator that appears in the electromagnetic wave equation is difficult to invert numerically, and this cannot be done iteratively. The addition of a higher order term that emphasizes the diagonal terms in the operator may help the solution of the problem, and the new equation should be solvable by an iterative algorithm. The additional mode is suppressed by suitable boundary conditions.

1. Introduction

The **curl curl** operator that appears in the electromagnetic wave equation

is difficult to invert numerically, as it is well known [Weitzner, 1984; Jaeger *et al*, 1986; Batchelor *et al*, 1988]; in effect, the **curl** has a large null space: all the functions that are gradients. In the vacuum we can consider the eigenvalue equation (with $\omega^2/c^2 = \lambda$) **curl curl** $\mathbf{E} = \lambda\,\mathbf{E}$; this equation has the degenerated eigenvalue $\lambda = 0$, and the associated eigenfunctions are those with **div** $\mathbf{E} \neq 0$, that is, all the electrostatic modes. Numerically, the array that has to be inverted has diagonal elements that are smaller than some off-diagonal terms; this imbalance prevents the straightforward use of iterative solving methods. Another inconvenience, related to the existence of the degenerated zero eigenvalue, is the eventual appearance of polluting modes when the three components of the electric field are represented with the same finite element basis functions [Lamalle, 1988].

On the other hand, the Laplacian operator ∇^2 does not present any of these difficulties: the diagonal elements are dominant, and it is pollution-free (under the conditions mentioned above). The fact that the difference between the Laplacian and **curl curl is grad div** suggests that adding a term of the form Λ **grad div**, with Λ a constant, to the **curl curl** operator could help in solving the equation, eliminating the degenerated zero eigenvalue. The solutions of the driven equation (frequency ω fixed by a source) will not be changed by the additional term if: a) the eigenvalues of the modified operator include all the non-zero eigenvalues of **curl curl**, and b) the new modes, corresponding to the additional finite eigenvalues, do not appear in the solution.

In Section 2 we present first such an operator in the vacuum, where it is easier to follow the steps that lead to the introduction of the new term, and we introduce later the more general case of a plasma, with a dielectric tensor.

And in Section 3 we discuss the numerical resolution of the modified equation and show some preliminary results.

2. Theory

2.1 The vacuum.

The electromagnetic wave equation in vacuum is

$$\mathbf{curl\ curl}\,\mathbf{E} = \frac{\omega^2}{c^2}\mathbf{E} \tag{1a}$$

and, for a perfectly conducting boundary $\partial\Omega$, the boundary conditions are

$$\mathbf{n}\times\mathbf{E} = 0 \qquad \text{on } \partial\Omega \tag{1b}$$

where $\mathbf{n}$ is the unit vector normal to the surface $\partial\Omega$; more generally,

$$\mathbf{n}\times\mathbf{E} \quad \text{continuous across } \partial\Omega. \tag{1c}$$

In the case of 1-D problems, Eq. (1a) is a fourth order system of three ordinary differential equations, and only needs four boundary conditions; for example, those given by (1b) or (1c). We will consider ω as a fixed parameter, given by the source (an antenna) added to Eq. (1a).

For $\omega \neq 0$, Eq. (1a) implies $\mathbf{div}\,\mathbf{E} = 0$. If we use the identity $\mathbf{curl\ curl} = -\nabla^2 + \mathbf{grad\ div}$, we can write the system of equations

$$-\nabla^2\mathbf{E} = \frac{\omega^2}{c^2}\mathbf{E} \tag{2a}$$

$$\mathbf{div}\,\mathbf{E} = 0 \tag{2b}$$

$$\mathbf{n}\times\mathbf{E} \text{ continuous across } \partial\Omega. \tag{2c}$$

equivalent to (1) for $\omega \neq 0$. As this system is exactly equivalent to (1), it is of fourth order in the 1-D case, even if Eq. (2a) is by itself a system of sixth order.

When we take the divergence of Eq. (2a), we see that

$$\left(\nabla^2 + \frac{\omega^2}{c^2}\right)\psi = 0 \tag{3}$$

where $\psi = \mathbf{div}\,\mathbf{E}$. If $\psi = 0$ on the boundaries, Eq. (3) guarantees that $\psi = \mathbf{div}\,\mathbf{E}$ is zero everywhere if ω is not an eigenvalue of (3). Thus we can replace Eq. (2b) by a *boundary condition*, and we obtain a system of equations that gives the same solutions as (1) when $\omega \neq 0$ is not an eigenvalue of (3):

$$-\nabla^2\mathbf{E} = \frac{\omega^2}{c^2}\mathbf{E} \tag{4a}$$

$$\mathbf{div}\,\mathbf{E} = 0 \quad \text{on } \partial\Omega \tag{4b}$$

$$\mathbf{n}\times\mathbf{E} \text{ continuous across } \partial\Omega. \tag{4c}$$

This is now a sixth order system in 1-D, and it needs six boundary conditions; the two additional conditions are given by $\mathbf{div}\,\mathbf{E} = 0$ on $\partial\Omega$.

Although we have succeeded in replacing the **curl curl** operator by the Laplacian, the system (4) is not satisfactory: the new additional non-zero eigenvalues of Eq. (4) (that is, those of Eq. (3)) are equal to the eigenvalues of (1). In effect, the eigenvalues of (1) — the dispersion relation — are

$$\omega^2/c^2 = k_x^2 + k_y^2 + k_z^2 \tag{5}$$

twice degenerated (two polarizations), if we assume the usual Fourier-style spatial dependence, whereas the eigenvalues of (3) are also given by (5). It would be much more desirable for the modified operator to have the new "unphysical" eigenvalues well separated from the "true" eigenvalues.

The replacement done to Eq. (1a) to obtain Eqs. (2) is equivalent to substracting **grad div E** from the left hand side of Eq. (1a). If we substract Λ **grad div E** , with Λ a *non-zero constant*, we obtain, for $\omega \neq 0$,

$$-\nabla^2 \mathbf{E} + \mathbf{grad\,div}\,(1-\Lambda)\,\mathbf{E} = \frac{\omega^2}{c^2}\mathbf{E} \tag{6a}$$

$$\mathbf{div}\,\mathbf{E} = 0 \tag{6b}$$

$$\mathbf{n}\times\mathbf{E} \text{ continuous across } \partial\Omega. \tag{6c}$$

The divergence of Eq. (6a) gives now

$$\left(\Lambda\nabla^2 + \frac{\omega^2}{c^2}\right)\psi = 0\,. \tag{7}$$

Thus, for $\omega \neq 0$ not an eigenvalue of (7), the sixth order system of equations

$$-\nabla^2 \mathbf{E} + \mathbf{grad\ div}\ (1-\Lambda)\,\mathbf{E} = \frac{\omega^2}{c^2}\mathbf{E} \tag{8}$$

or, equivalently,

$$\mathbf{curl\ curl\ E} - \Lambda\,\mathbf{grad\ div\ E} = \frac{\omega^2}{c^2}\mathbf{E} \tag{8'}$$

with the boundary conditions

$$\mathbf{div}\,\mathbf{E} = 0 \quad \text{on } \partial\Omega \tag{8b}$$

$$\mathbf{n} \times \mathbf{E} \quad \text{continuous across } \partial\Omega. \tag{8c}$$

has the same solutions as the original system (1). The new eigenvalues are now those of Eq. (7), that is,

$$\omega^2/c^2 = \Lambda\,(k_x^2 + k_y^2 + k_z^2) \tag{9}$$

and they may be separated from the original ones. In a 1-D problem, for example, where ω, k_y and k_z are given, the physical modes

$$k_x^2 = \omega^2/c^2 - (k_y^2 + k_z^2) \tag{10}$$

can be kept away from the unphysical modes

$$k_x^2 = (\omega^2/c^2)/\Lambda - (k_y^2 + k_z^2) \tag{11}$$

by a suitable choice of the value of Λ; if we are studying propagating modes ($k_x^2 > 0$), setting $\Lambda < 0$ makes the Λ-dependent modes evanescent. The amplitude of these modes, which are characterized by $\mathbf{div}\,\mathbf{E} \neq 0$, is set to zero by the boundary conditions.

As an added bonus, it is straightforward to verify [Llobet *et al*, 1990] that the modified system of equations is pollution-free.

2.2 The plasma.

In a plasma the electromagnetic wave equation becomes

$$\mathbf{curl\ curl\ E} = \frac{\omega^2}{c^2}\,\mathbf{D} \tag{12}$$

where $\mathbf{D} = \varepsilon\,\mathbf{E}$, ε being the dielectric tensor, which is a differential operator for hot plasmas. The boundary conditions are still given by (1b) for a perfect conductor, or (1c).

Now, **div E** is replaced by **div D**. For finite frequencies, Eq. (12) implies **div D** = 0. Substracting Λ **grad div D** from the left hand side we obtain,

$$\mathbf{curl\ curl\ E} - \Lambda\,\mathbf{grad\ div\ D} = \frac{\omega^2}{c^2}\mathbf{D} \tag{13a}$$

$$\mathbf{div\ D} = 0 \tag{13b}$$

$$\mathbf{n}\times\mathbf{E} \text{ continuous across } \partial\Omega. \tag{13c}$$

The divergence of Eq. (13a) gives

$$\left(\Lambda\nabla^2 + \frac{\omega^2}{c^2}\right)\psi = 0 \tag{14}$$

with $\psi = \mathbf{div\ D}$. Thus, for $\omega \neq 0$ not an eigenvalue of (14), the system of equations

$$\mathbf{curl\ curl\ E} - \Lambda\,\mathbf{grad\ div\ D} = \frac{\omega^2}{c^2}\mathbf{D} \tag{15a}$$

$$\mathbf{div\ D} = 0 \text{ on } \partial\Omega \tag{15b}$$

$$\mathbf{n}\times\mathbf{E} \text{ continuous across } \partial\Omega. \tag{15c}$$

has the same solutions as (12). In the cases of physical interest, this modified operator is two orders higher than the original one, as in the vacuum case, and it needs the two additional boundary conditions **div D** = 0.

As the dielectric tensor depends on ω, we cannot treat ω^2 as an eigenvalue, but we can still consider the dispersion relations of the two systems of equations. It is clear that the new modes are those described by Eq. (14), which is identical to Eq. (7). Thus, their dispersion relation is that of Eq. (7) and, like in the vacuum case,

$$\omega^2/c^2 = \Lambda\,(k_x^2 + k_y^2 + k_z^2). \tag{9}$$

It is somewhat surprising that these additional modes, obtained by the addition of a term that depends on the plasma dielectric tensor, and characterized by **div D** $\neq 0$, have a dispersion relation that does not depend at all on the plasma: they look like pure cavity modes.

3. Numerical resolution.

We have solved this Modified Electromagnetic Wave Equation (MEWE) using its operator in the 1-D slab global wave code ISMENE [Appert *et al,* 1987]. The vacuum and the cold plasma cases are a success, as the results are even better than those from ISMENE. On the other hand, in the hot plasma case, the converged results are the same, but the convergence is somewhat slower.

The ISMENE code uses a finite element method to solve the equations. The equation to be solved is multiplied by a test function, and integrated over the domain; the details can be found in the paper by Appert *et al*, 1986. Only the relevant calculations are presented in what follows.

3.1 The vacuum.

Multiplying Eq. (8') by the arbitrary test function $\mathbf{F}$ we have, after integrating by parts over the domain Ω,

$$\int_{\Omega} dV \left[(\mathbf{curl}\, \mathbf{F}) \cdot (\mathbf{curl}\, \mathbf{E}) + \Lambda (\mathbf{div}\, \mathbf{F})(\mathbf{div}\, \mathbf{E}) - \frac{\omega^2}{c^2} \mathbf{F} \cdot \mathbf{E} \right] =$$

$$= \int_{\partial\Omega} dS\, \mathbf{n} \cdot [\mathbf{F} \times \mathbf{curl}\, \mathbf{E} + \Lambda \mathbf{F} (\mathbf{div}\, \mathbf{E})] \qquad (16)$$

The boundary condition $\mathbf{div}\, \mathbf{E} = 0$ allows us to drop the second term in the surface integral. If the boundary is a perfect conductor, the essential condition (1b) $\mathbf{n} \times \mathbf{E} = 0$ permits to drop also the first term [Strang and Fix, 1973]; but we may study more general regions of space (for example, a region near an antenna) and evaluate the first term with matching conditions (8c). More specifically, the terms in the integrand of the right hand side are

$$[F_x \Lambda (\mathbf{div}\, \mathbf{E}) + F_y (E_y' - i k_y E_x) + F_z (E_z' - i k_z E_x)]\, \mathbf{e}_x \qquad (17)$$

In this case (the vacuum) it is trivial to evaluate these terms (proportional to B_z and B_y), as the fields are continuous, and we can write these terms as functions of the tangential components of the electric field at the interface and of the source characteristics.

It is appropriate to notice that the surface terms in (17) provide the ability to impose three natural boundary conditions, as there are three free test function parameters (F_x, F_y and F_z at the surface). The three boundary conditions are the continuity of the tangential components of the electric field

(two conditions), and **div E** = 0, which can be imposed separately by dropping the Λ-dependent surface term. The matching conditions obtained by integrating Eq. (8') across the interface (vacuum-vacuum in this case), are that the factors of F_x, F_y and F_z in (17) have to be continuous; in this case, the use of these conditions does not bring anything new.

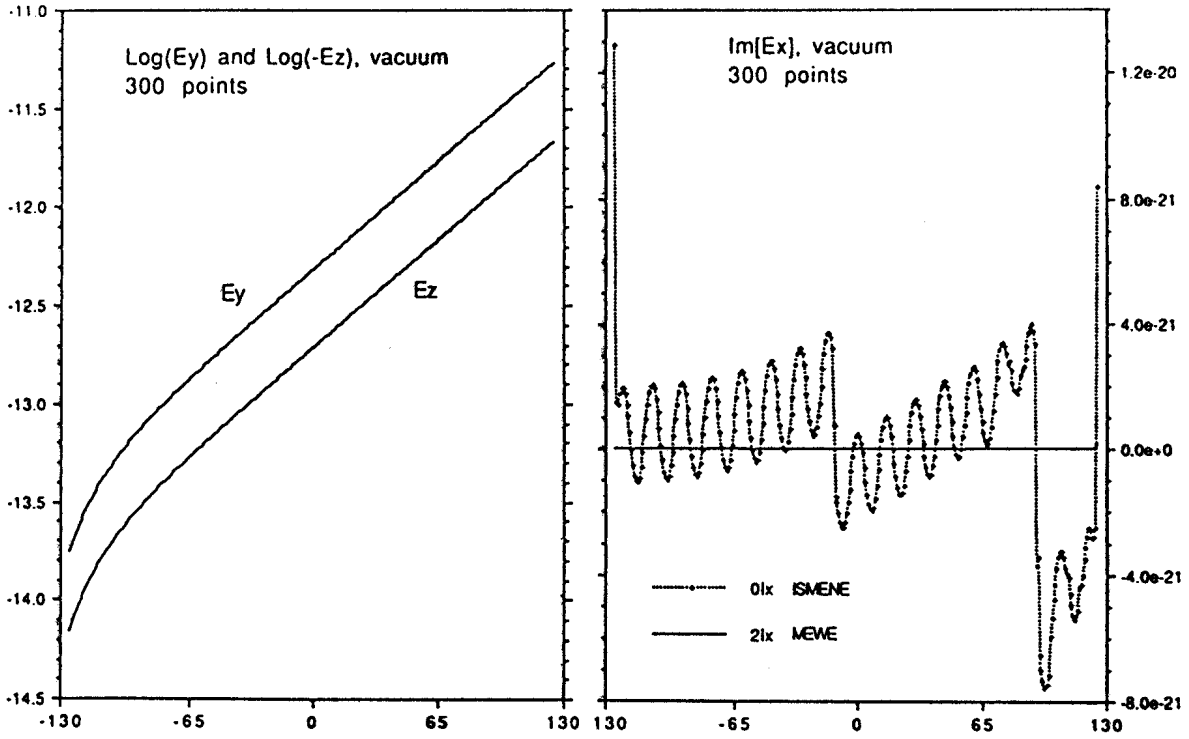

Figure 1. Electric field in the vacuum case.

Fig. 1 shows the results in the case of an evanescent wave (240 MHz), launched by an antenna parallel to the y-z plane, so that E_x should be zero. The domain extends from $x_l = -125$ cm to $x_r = 125$ cm, with the antenna at $x_a = 131.5$ cm and metallic walls at $x = \pm 138$ cm; the y and z components of the wave vector are $k_y = 0.02$ cm^{-1} and $k_z = 0.05$ cm^{-1} (these values, except for the frequency, apply to all the cases presented in this paper). The left panel shows (the logarithm of) the tangential components of the electric field; the results of MEWE and of ISMENE agree to more than five digits with each other and with the analytical solution. On the other hand, E_x is not zero: its

source is the finite value of the combination $k_y E_y + k_z E_z$ at the boundary, which should be exactly zero, but the two terms cancel each other "only" up to 10^{-5}. It is clear that ISMENE's result is good enough, but the fact that MEWE improves it is encouraging. The improvement is much more remarkable in the cases where ISMENE suffers from pollution.

These results were obtained using cubic Hermite finite elements, which guarantee the continuity of the solution and of the first derivative, and only these quantities are used in the volume integral and in the surface integral. Linear elements could be used in ISMENE, as the discontinuities in the first derivative do not matter in the volume integral, and the surface integral can be written, as explained above, as function only of the solution at the boundary, not of its derivatives. MEWE needs to take into account the div E term, even if it is to dismiss it naturally; although the first derivative is discontinuous at the mesh points, it is finite and its one-sided limit exists, and this is what is needed.

3.2 The plasma.

In the plasma the dielectric tensor is a differential operator. To the second order of the expansion in powers of the Larmor radii, it is of second order, and has this structure in 1-D [Martin and Vaclavik, 1987]:

$$\varepsilon = \frac{d}{dx}\,\alpha\,\frac{d}{dx} + \beta\,\frac{d}{dx} + \frac{d}{dx}\,\beta^{+} + \gamma \qquad (18)$$

with

$$\alpha = \begin{pmatrix} \alpha_{xx} & \alpha_{xy} & 0 \\ -\alpha_{xy} & \alpha_{yy} & 0 \\ 0 & 0 & \alpha_{zz} \end{pmatrix}, \tag{18a}$$

$$\beta = \begin{pmatrix} 0 & \beta_{xy} & \beta_{xz} \\ 0 & 0 & \beta_{yz} \\ 0 & 0 & 0 \end{pmatrix}, \quad \beta^{+} = \begin{pmatrix} 0 & 0 & 0 \\ \beta_{xy} & 0 & 0 \\ \beta_{xz} & -\beta_{yz} & 0 \end{pmatrix}, \tag{18b}$$

and γ given by functions of ω, k_y, k_z, the plasma parameters (density, temperature, magnetic field) and their derivatives, assuming $\mathbf{B} = B(x)\,\mathbf{e}_z$.

Multiplying Eq. (15) by the test function $\mathbf{F}$ and integrating once by parts we obtain the analog of the Eq. (16)

$$\int_{\Omega} dV\,[\,(\mathbf{curl}\,\mathbf{F})\cdot(\mathbf{curl}\,\mathbf{E}) + \Lambda(\mathbf{div}\,\mathbf{F})(\mathbf{div}\,\mathbf{D}) - \frac{\omega^2}{c^2}\mathbf{F}\cdot\mathbf{D}\,] =$$

$$= \int_{\partial\Omega} dS\,\mathbf{n}\cdot[\,\mathbf{F}\times\mathbf{curl}\,\mathbf{E} + \Lambda\,\mathbf{F}\,(\mathbf{div}\,\mathbf{D})\,] \tag{19}$$

with the boundary condition

$$\mathbf{div}\,\mathbf{D} = 0 \quad \text{on}\,\partial\Omega. \tag{19'}$$

Now the term **div D** has third derivatives. Third derivatives of cubic Hermite finite elements are not only discontinuous but singular (δ function) at the mesh points; they must be avoided [Strang and Fix, 1973, p. 62]. Integrating by parts once more leads to

$$\int_{x_l}^{x_r} dx \left[(\mathbf{curl}\,\mathbf{F})\cdot(\mathbf{curl}\,\mathbf{E}) - \Lambda\,\mathbf{grad}\,(\mathbf{div}\,\mathbf{F})\cdot\varepsilon\cdot\mathbf{E} - \right.$$

$$\left. - \frac{\omega^2}{c^2}\mathbf{F}\cdot\left(\gamma + \beta\frac{d}{dx}\right)\cdot\mathbf{E} + \frac{\omega^2}{c^2}\left(\frac{d}{dx}\mathbf{F}\right)\cdot\left(\beta^+ + \alpha\frac{d}{dx}\right)\cdot\mathbf{E} \right] = \tag{20}$$

$$= \left[[\,\mathbf{F}\times\mathbf{curl}\,\mathbf{E} + \Lambda\,\mathbf{F}\,(\mathbf{div}\,\mathbf{D}) - \Lambda\,(\mathbf{div}\,\mathbf{F})\,\mathbf{D}\,]_x + \frac{\omega^2}{c^2}\mathbf{F}\cdot\left(\beta^+ + \alpha\frac{d}{dx}\right)\cdot\mathbf{E} \right]_{x_l}^{x_r}$$

with the boundary condition

$$\mathbf{div}\,\mathbf{D} = 0 \quad \text{at } x_l \text{ and } x_r. \tag{20'}$$

The surface term in (20) is

$$\begin{aligned} & F_x\,[\Lambda\,(\mathbf{div}\,\mathbf{D}) + (\omega^2/c^2)\,(\alpha_{xx}E_x' + \alpha_{xy}E_y')] - \\ & - F_x'\,\Lambda\,D_x + \\ & + F_y\,[(E_y' - i\,k_y\,E_x) + (\omega^2/c^2)\,(\beta^+\cdot\mathbf{E} + \alpha\cdot\mathbf{E}')_y + i\,k_y\,\Lambda\,D_x] + \\ & + F_z\,[(E_z' - i\,k_z\,E_x) + (\omega^2/c^2)\,(\beta^+\cdot\mathbf{E} + \alpha\cdot\mathbf{E}')_z + i\,k_z\,\Lambda\,D_x]\,. \end{aligned} \tag{21}$$

We now have to impose the three boundary conditions: continuity of tangential components of **E**, and **div D** = 0. But we need four conditions to have a unique solution. The fourth boundary condition can be obtained from the matching conditions; integrating Eq. (15) across the interface gives that the combinations

$$\Lambda\,(\mathbf{div}\,\mathbf{D}) + (\omega^2/c^2)\,(\alpha_{xx}E_x' + \alpha_{xy}E_y') \tag{22a}$$

$$(\omega^2/c^2)\,(\beta^+\cdot\mathbf{E} + \alpha\cdot\mathbf{E}')_y + (\mathbf{curl}\,\mathbf{E})_z \tag{22b}$$

$$(\omega^2/c^2)\,(\beta^+\cdot\mathbf{E} + \alpha\cdot\mathbf{E}')_z - (\mathbf{curl}\,\mathbf{E})_y \tag{22c}$$

are continuous, so they can be replaced by their values in the vacuum. Then

we have (22a) = 0, and this is the fourth condition.

The two boundary conditions **div D** = 0 and (22a) = 0 can be imposed by dropping the first surface term, corresponding to F_x (natural condition) and setting

$$\alpha_{xx} E_x' + \alpha_{xy} E_y' = 0 \tag{23}$$

(essential condition); this combination ensures that **div D** = 0. It is clear that this condition cannot be imposed essentially, due to the singularity of the third derivative.

We can use the continuity of (22b) and (22c) to simplify the expression of the surface terms, as their values in the vacuum can be expressed as functions of the tangential fields alone. The expression of the surface term is

$$[\mathbf{F} \times \mathbf{curl}\, \mathbf{E}_{vac}]_x - \Lambda (\mathbf{div}\, \mathbf{F})\, D_x \quad . \tag{24}$$

The last step is to obtain an expression for D_x at the inside surface of the boundary, to evaluate (24); in general, for a hot plasma with finite density and temperature at the edge, there are surface currents and charge, which make D_x discontinuous. There are two ways to calculate D_x : the first one is to use $D_x = (\varepsilon \cdot \mathbf{E})_x$; this implies the use of second derivatives, which exist only as one-sided limit. The second way is to realize that when **div D** = 0, **D** is proportional to **curl B**, so the jump of D_x can be written as a function of the jumps of B_y and B_z, which we know from the integration across the interface of Eq. (15) mentioned above. The result is

$$D_x = (E_x)_{vac} - i\,\mathbf{k}\cdot\left(\beta^{+} + \alpha\frac{d}{dx}\right)\cdot\mathbf{E} \qquad (25)$$

where $\mathbf{k}$ has only y and z components; the vacuum value of E_x is computed from the tangential components.

It turns out that if (25) is used in all the occurrences of D_x in the surface term the results are wrong; if at least one term (on each boundary) is evaluated from $(\varepsilon \cdot \mathbf{E})_x$, the results are correct. This occurs even in the vacuum, where the choice is to get E_x from the solution directly, or from the tangential components. Thus, even if both ways appear in principle to be correct, the second one must be a computational crime.

Following this method, the results obtained are indeed quite good. We have focussed most of our efforts on one test case: a JET-size deuterium plasma with parabolic density and temperature profiles, launching a fast wave (60 MHz) above $2\omega_{ci}$. More specifically, the parameters at the center are: $n_0 = 4.5 \times 10^{13}$ cm^{-3}, $T_e = T_i = 2$ keV, $B_0 = 3.4$ T. Fig. 2 shows the real and imaginary parts of E_y (we use E_y as diagnostic, as its behaviour is representative of all the other components: its real part is large, and its converged value agrees very well with ISMENE, while its imaginary part is small, and shows the largest relative error). With 300 points the results agree to better than 1-2%, and the difference between the results of ISMENE and MEWE wouldn't be appreciated in the figure, but as it can be seen in Fig. 3, which presents the solutions near the right edge, it is clear that the MEWE solution is not satisfactory: it shows a sharp bend.

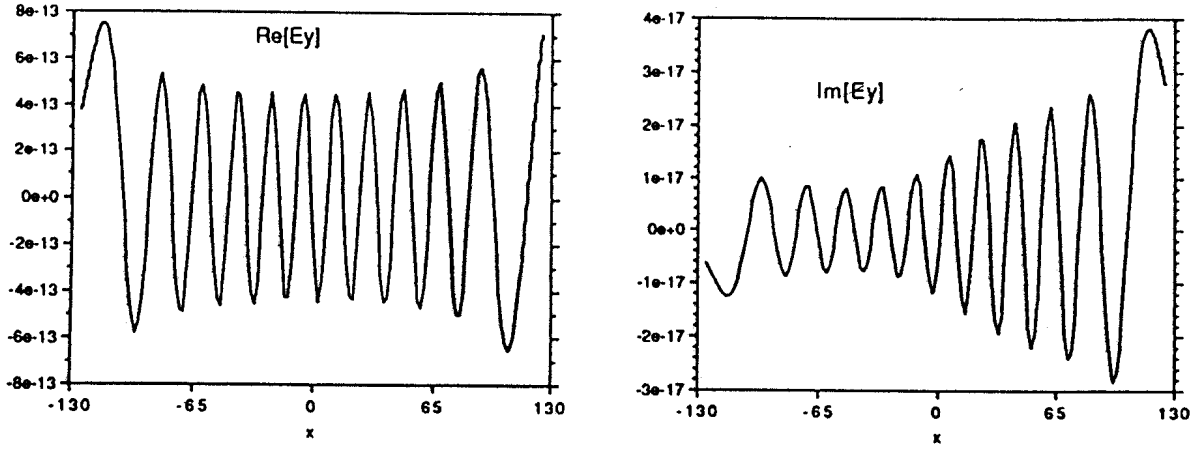

Figure 2. Real and imaginary parts of E_y in a plasma (fast wave).

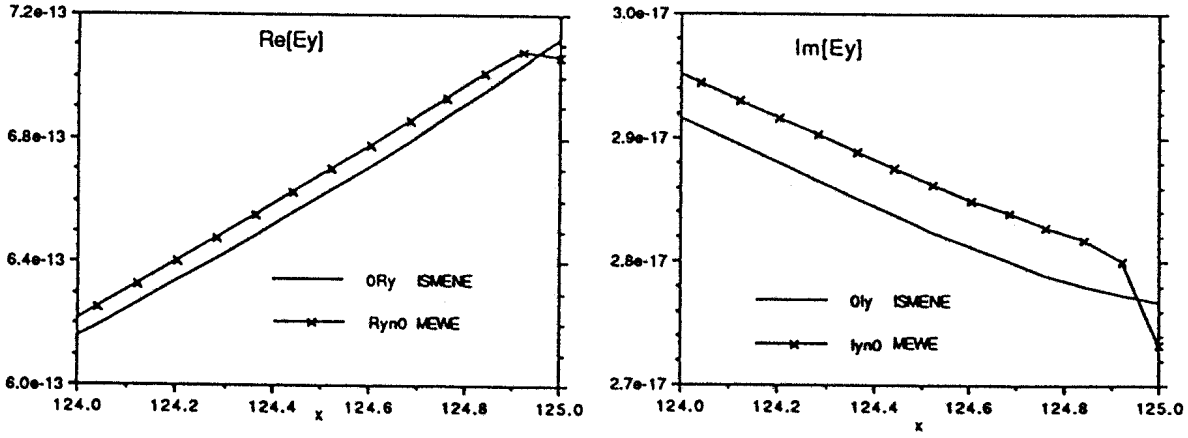

Figure 3. E_y near the right boundary; ISMENE and MEWE solutions.

As this "feature" seems to be localized in the last interval, we can try to pack more points near the edge. Thus to add N_a additional points in the last interval of length H we place the first at H/2 from the edge, the next at H/4, the next at H/8, etc. With this packing, the behaviour of the solution near the

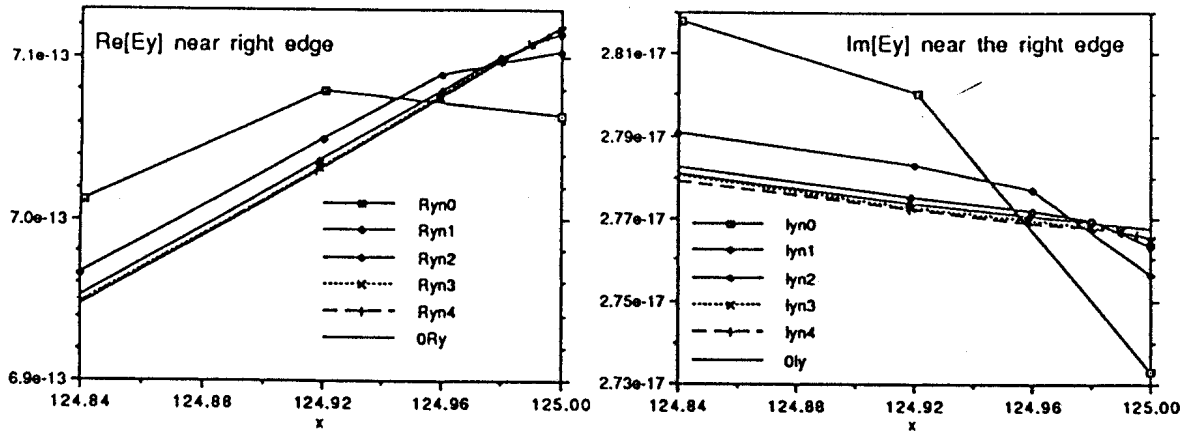

Figure 4. MEWE solutions with different number of additional points near the edge. The ISMENE solutions are labeled 0Ry and 0Iy.

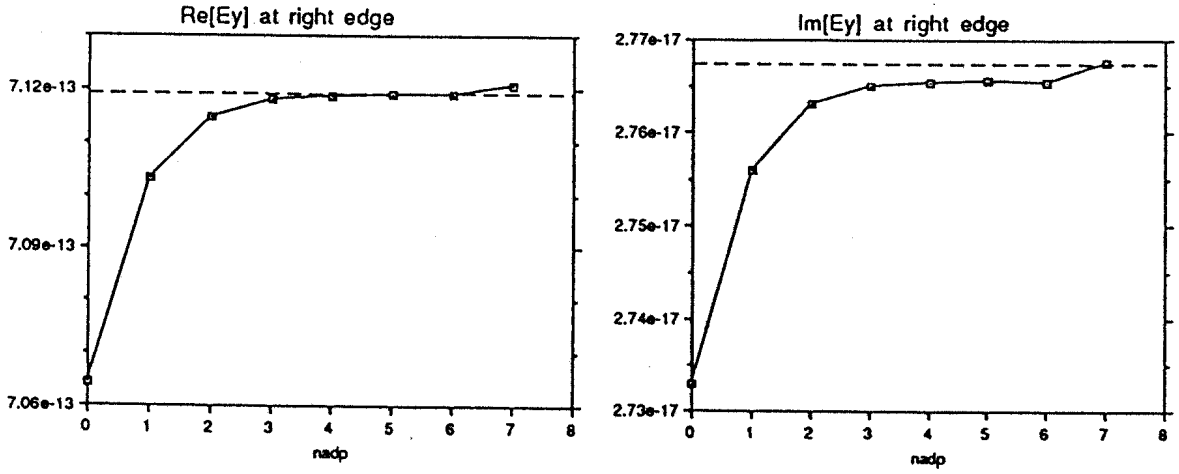

Figure 5. Edge values of E_y as a function of the number of additional points.

edge becomes acceptable, as shown in Fig. 4, where we plot the fields for a different number of additional points (0 to 4) and the ISMENE solution. How many points should be inserted? In Fig. 5 we show the field values at the edge versus the number of additional points. It is a general feature that as this number increases, the solutions tend first to a value, but later diverge

(this behaviour recalls the asymptotic expansions). In this case, the "optimum" value, which should be determined from all the components of the solution, seems to be 5. When we use 600 points, the optimum value is 4, and for 1200 is 3. It looks like there is an optimum value for the smallest interval at the edge; it turns out to be of the order of the smallest physical distance imbedded in the dielectric tensor, which is the electron Larmor radius, or the Debye length. This distance is much smaller than any of the wavelengths derived from a WKB analysis.

With this "recipe", the convergence of the fields at the edge of MEWE, in the "optimum" series (300,5), (600,4), (1200,3) is approximately in N^{-2} (ISMENE converges as N^{-4}). We certainly expect a slower convergence in the modified equation, as second derivatives are used, which are poorly represented (they are discontinuous). An additional reason to explain the relative poor convergence is the (in)famous boundary condition **div D** = 0; the fact that third derivatives are not properly represented by cubic Hermite elements may explain the need for the "ad hoc" introduction of points near the edge and the slower convergence.

4. Conclusions.

The modified electromagnetic equation introduced in this paper has a series of theoretical advantages with respect to the classical equation: it has no degenerated zero eigenvalue, is pollution-free, and has a more dominant diagonal. In the dispersion relation the new modes can be factored out, and crossings with the physical branches may be avoided. The numerical resolution of this equation poses some practical difficulties, mostly in the

evaluation of the new surface terms and in the implementation of the **div D** = 0 at the boundary. We have found a way to solve these problems, and the numerical solutions of the modified equation converge to the classical solutions, though more slowly.

The main goal of building this modified equation is to allow the use of iterative methods, which seem not to be of use in the classical equation. We have not yet tried any of these methods, but plan to do so in the near future.

Acknowledgements

This work was partly supported by the Swiss National Science Foundation.

References

Appert, K., T. Hellsten, J. Vaclavik, and L. Villard, "Textbook finite element methods applied to linear wave propagation problems involving conversion and absorption", Computer Phys. Commun. **40** (1986) 73-93.

Appert, K., T. Hellsten, H. Lütjens, O. Sauter, J. Vaclavik, and L. Villard, "The physics of wave-coupling in low-frequency plasma heating", in *Proceedings of the International Conference on Plasma Physics, (Kiev, URSS, 1987)* Invited Papers, edited by A.G. Sitenko (World Scientific, Singapore, 1987), 1230-1255.

Batchelor, D.B., E.F. Jaeger, and H. Weitzner, " 2D Full Wave Modeling of

ICRF with Finite $E_{||}$", in *Proceedings of the joint Varenna-Lausanne international workshop on the Theory of Fusion Plasmas (Chexbres, Switzerland, 1988)* edited by J. Vaclavik, F. Troyon and E. Sindoni (Editrice Compositori, Bologna, 1989), 691-698.

Jaeger, E.F., D.B. Batchelor, H. Weitzner, and J.H. Whealton, "ICRF wave propagation and absorption in tokamak and mirror magnetic fields – a full-wave calculation", Computer Phys. Commun. **40** (1986) 33-64.

Lamalle, P.U., "Finite element discretization of the ICRF wave equation", in *Proceedings of the joint Varenna-Lausanne international workshop on the Theory of Fusion Plasmas (Chexbres, Switzerland, 1988)* edited by J. Vaclavik, F. Troyon and E. Sindoni (Editrice Compositori, Bologna, 1989), 699-706.

Llobet, X., K. Appert, A. Bondeson, and J. Vaclavik, "On spectral pollution", Computer Phys. Commun. **59** (1990) 199-216.

Martin, T., and J. Vaclavik, "Dielectric tensor operator of a nonuniformly magnetized inhomogeneous plasma", Helv. Physica Acta **60** (1987) 471-479.

Strang, G. and G.J. Fix, *"An Analysis of the Finite Element Method"* (Prentice Hall, Englewood Cliffs, NJ, 1973).

Weitzner, H., "Wave Propagation in a Plasma Based on the Cold Plasma Model", Report MF-103, Courant Inst. of Math. Sciences, New York Univ., New York, N.Y., August 1984.

Local Absorption Of Linear Electromagnetic Waves In Uniformly Magnetized, Inhomogeneous Plasmas

A. Jaun and J. Vaclavik

Centre de Recherches en Physique des Plasmas
Association Euratom - Confédération Suisse
Ecole Polytechnique Fédérale de Lausanne
21, av. des Bains – CH-1007 Lausanne/Switzerland

A general expression for local power absorption of small amplitude electromagnetic fields in a hot, uniformly magnetized plasma is obtained starting from Vlasov-Maxwell equations. Using a transformation to Lagrangian coordinates, the power is calculated without introducing the flux due to particle streaming, and corresponds to the local exchange of energy between the wave and the plasma.
Assuming the Larmor radii of the species to be small compared with the characteristic scale length of the fields and the equilibrium quantities such as density and temperature, an expansion to second order is carried out. This results in an explicit expression for local power absorption in a 2-D plasma, which takes into account the effects due to density and temperature gradients.

1 Introduction

One way commonly used to raise the temperature in a fusion device is to launch electromagnetic waves into the plasma, the energy of which may then be converted into electron and ion heat according to the well known wave-particle processes such as Landau damping, cyclotron damping and transit time magnetic pumping.

In order to control the heating, it is important to know exactly where the energy is dissipated. Such deposition profiles depend on the characteristics of the wave and on the local properties of the plasma along its trajectory. Standing waves created by partial reflections inside the plasma, eigenmode oscillations and strongly damped waves

are field patterns commonly encountered in RF heating, for which a WKB description often does not hold.

In this paper, an expression for the local power absorption density is obtained in terms of an arbitrary linear EM field in a hot, uniformly magnetized plasma, taking into account effects due to density and temperature gradients.

2 Energy Balance in Lagrangian Coordinates

A general formulation for the local power absorption has recently been obtained directly from fundamental principles (McVey *et al.*, 1985; Vaclavik and Appert, 1987). Using a transformation into Lagrangian coordinates $(\boldsymbol{x}',\boldsymbol{v}',t')$, the energy moment of the Vlasov equation is first written without introducing the flux of energy due to thermal motion of particles. With the lowest frequency involved in the expression for power absorption being $|\omega-\Omega_c|$, it has been shown that an average in time over the scale $\Delta\tau \sim |\omega-\Omega_c|^{-1}$ must be carried out in conjunction with an average in space along the direction of magnetostatic field $\boldsymbol{B}_0 = B_0\,\boldsymbol{e}_z$as the particles will then move in the same direction by a distance $\lambda_\parallel = \Delta\tau v_\parallel$. Here $v_\parallel$ is a typical particle velocity component parallel to the magnetic field, Ω_c the cyclotron frequency of the species and ω the frequency of the wave. All this yields an expression for the power absorption in terms of the electric field components $\boldsymbol{E}$ of the electromagnetic field and the linear term f_1 in the expansion of the distribution function f in powers of $\boldsymbol{E}$:

$$P_L(\boldsymbol{x}_\perp) = \frac{q}{2}\int d\boldsymbol{v}\; Re < \boldsymbol{E}^*(\boldsymbol{x}'_\perp)\cdot\boldsymbol{v}' f_1(\boldsymbol{x}'_\perp,\boldsymbol{v}') >_{t'} . \tag{1}$$

The trajectories of particles with charge q and mass m are given by

$$\begin{aligned}
&\boldsymbol{x}'_\perp = \boldsymbol{x}_\perp + \frac{v_\perp}{\Omega_c}\left[(\sin\alpha - \sin\alpha')\boldsymbol{e}_x + (\cos\alpha' - \cos\alpha)\boldsymbol{e}_y\right],\\
&\boldsymbol{v}' = v_\perp(\cos\alpha'\boldsymbol{e}_x + \sin\alpha'\boldsymbol{e}_y) + v_z\boldsymbol{e}_z,\\
&\alpha' = \alpha + \Omega_c(t-t'), \quad v_\perp = (v_x^2+v_y^2)^{1/2}, \quad \alpha = \tan\frac{v_y}{v_x},
\end{aligned} \tag{2}$$

and depend exclusively on the static magnetic field $\boldsymbol{B}_0$ so that the only term in (1) carrying information about inhomogeneity is $f_1(\boldsymbol{x}'_\perp,\boldsymbol{v}')$.

3 Linear perturbation of the distribution

By an integration of the Vlasov equation over unperturbed orbits, f_1 is related to the equilibrium distribution which is known to have a dependency of the form $f_0(X = x + v_y/\Omega_c, Y = y - v_x/\Omega_c, v_\parallel, v_\perp)$, all four parameters being constants of motion. For practical use, f_0 is assumed maxwellian

$$f_0(\boldsymbol{X}_\perp, v_\perp, v_\parallel) \equiv f_M = \pi^{-3/2}\, n_0\, v_t^{-3} \exp\left[-\frac{(v_\perp^2 + v_\parallel^2)}{v_t^2}\right], \qquad v_t = \left(\frac{2T}{m}\right)^{1/2}, \tag{3}$$

where $n_0(\boldsymbol{X}_\perp)$ and $T(\boldsymbol{X}_\perp)$ refer to the plasma density and temperature. Upon using the Fourier transforms

$$\{\boldsymbol{E}(\boldsymbol{x}_\perp), f_1(\boldsymbol{x}_\perp, \boldsymbol{v})\} = \int d\boldsymbol{k}_\perp \exp\left[i(\boldsymbol{k}_\perp \cdot \boldsymbol{x}_\perp)\right] \{\boldsymbol{E}(\boldsymbol{k}_\perp), f_1(\boldsymbol{k}_\perp, \boldsymbol{v})\}, \tag{4}$$

$$f_0(\boldsymbol{X}_\perp, \boldsymbol{v}) = \int d\boldsymbol{q}_\perp \exp\left[iq_x(x + v_y/\Omega_c)\right] \exp\left[iq_y(y - v_x/\Omega_c)\right] f_0(\boldsymbol{q}_\perp, v_\perp, v_\parallel), \tag{5}$$

we obtain

$$\begin{aligned} f_1(\boldsymbol{k}, \boldsymbol{v}, \omega) \;=\; & \exp\left[\frac{i}{\Omega_c}(\boldsymbol{k} \times \boldsymbol{v}) \cdot \boldsymbol{e}_z\right] \sum_\ell \exp[-i\ell\alpha] \\ & \times \int d\boldsymbol{q}_\perp \exp[i\ell\varphi_{k-q}]\, \frac{-iq/m}{(\omega - k_\parallel v_\parallel - \ell\Omega_c)} \\ & \times \boldsymbol{A}_\ell(\boldsymbol{k}, \boldsymbol{q}_\perp, v_\perp, v_\parallel, \omega) \cdot \boldsymbol{E}(\boldsymbol{k}_\perp - \boldsymbol{q}_\perp), \end{aligned} \tag{6}$$

$$\begin{aligned} A_{\ell,x} \;=\; & \left\{\left(\frac{-2v_\perp}{v_t^2}\right)\left[\frac{\ell}{\Delta\xi} J_\ell(\Delta\xi)\cos(\varphi_{k-q}) - iJ_\ell'(\Delta\xi)\sin(\varphi_{k-q})\right]\right. \\ & + \frac{i}{\Omega_c} J_\ell(\Delta\xi)\left[\frac{k_\parallel v_\parallel}{\omega} - 1\right] q_y \\ & + i\left[q_y \sin(\varphi_{k-q}) + q_x \cos(\varphi_{k-q})\right] \frac{\ell}{\omega} J_\ell(\Delta\xi)\sin(\varphi_{k-q}) \\ & \left. + i\left[q_y \cos(\varphi_{k-q}) - q_x \sin(\varphi_{k-q})\right] i\frac{\Delta\xi}{\omega} J_\ell'(\Delta\xi)\sin(\varphi_{k-q})\right\} f_M, \end{aligned} \tag{7}$$

$$
\begin{aligned}
A_{\ell,y} \;=\; & \left\{\left(\frac{-2v_\perp}{v_t^2}\right)\left[\frac{\ell}{\Delta\xi}J_\ell(\Delta\xi)\sin(\varphi_{k-q}) + iJ'_\ell(\Delta\xi)\cos(\varphi_{k-q})\right]\right. \\
& - \frac{i}{\Omega_c}J_\ell(\Delta\xi)\left[\frac{k_\parallel v_\parallel}{\omega} - 1\right]q_x \\
& - i\left[q_y\sin(\varphi_{k-q}) + q_x\cos(\varphi_{k-q})\right]\frac{\ell}{\omega}J_\ell(\Delta\xi)\cos(\varphi_{k-q}) \\
& \left. - i\left[q_y\cos(\varphi_{k-q}) - q_x\sin(\varphi_{k-q})\right]i\frac{\Delta\xi}{\omega}J'_\ell(\Delta\xi)\cos(\varphi_{k-q})\right\} f_M,
\end{aligned}
\tag{8}
$$

$$
\begin{aligned}
A_{\ell,z} \;=\; & \left\{\left(\frac{-2v_\parallel}{v_t^2}\right)J_\ell(\Delta\xi)\right. \\
& \left. - i\left[q_y\cos(\varphi_{k-q}) - q_x\sin(\varphi_{k-q})\right]\left[\frac{|\boldsymbol{k}_\perp - \boldsymbol{q}_\perp|v_\parallel}{\omega\Omega_c}\right]J_\ell(\Delta\xi)\right\} f_M,
\end{aligned}
\tag{9}
$$

$$
\Delta\xi = \frac{v_\perp}{\Omega_c}|\boldsymbol{k}_\perp - \boldsymbol{q}_\perp|, \qquad \tan\varphi_{k-q} = \left(\frac{k_y - q_y}{k_x - q_x}\right), \tag{10}
$$

which is equivalent to a similar expression derived by Yasseen and Vaclavik (1986) with another method. J_ℓ and J'_ℓ are the Bessel function and its derivative. In order to satisfy causality, the frequency ω is assumed to have a small positive imaginary part.

4 General expression for power absorption

After substitution of (2) and (6) into (1), exponentials of Lagrangian quantities are expanded according to

$$
\exp(ia\sin b) = \sum_\ell J_\ell(a)\exp(i\ell b), \tag{11}
$$

and the average over time is carried out. Further use of Graf's summation theorem for Bessel functions (Gradshteyn, Ryzhik, 1965)

$$
\mathcal{J}_\ell(\boldsymbol{k}_\perp - \boldsymbol{q}_\perp) = \sum_n \mathcal{J}_{\ell+n}(\boldsymbol{k}_\perp)\mathcal{J}^*_n(\boldsymbol{q}_\perp), \qquad \mathcal{J}_\ell(\boldsymbol{k}_\perp) = J_l(\frac{k_\perp v_\perp}{\Omega_c})\exp(i\ell\varphi_k), \tag{12}
$$

finally yields a general form of the local power absorption density in terms of the local properties in the plasma:

$$P_L(\boldsymbol{x}_\perp) = P^{(1)} + P^{(2)}, \tag{13}$$

$$\begin{aligned}
P^{(1)} &= \frac{q^2}{2m} Im \int d\boldsymbol{v} \sum_\ell (\omega - \ell\Omega_c - k_\parallel v_\parallel)^{-1} \int d\boldsymbol{k}_\perp d\boldsymbol{k}'_\perp d\boldsymbol{q}_\perp \exp\left(i\ell[\varphi_k - \varphi_{k\prime}]\right) \\
&\quad \times \exp\left(i[\boldsymbol{k}_\perp - \boldsymbol{k}'_\perp] \cdot \boldsymbol{x}_\perp\right) \exp(i\boldsymbol{q}_\perp \cdot \boldsymbol{x}_\perp) J_0\left(\frac{v_\perp}{\Omega_c} |\boldsymbol{k}'_\perp - \boldsymbol{k}_\perp - \boldsymbol{q}_\perp|\right) \\
&\quad \times [\boldsymbol{B}_\ell(\boldsymbol{k}_\perp, v_\perp, v_\parallel) \cdot \boldsymbol{E}(\boldsymbol{k}_\perp)](-\frac{2}{v_t^2}) f_M(\boldsymbol{q}_\perp, v_\parallel, v_\perp) \left[\boldsymbol{B}_\ell(\boldsymbol{k}'_\perp, v_\perp, v_\parallel) \cdot \boldsymbol{E}(\boldsymbol{k}'_\perp)\right]^*, \\
P^{(2)} &= \frac{q^2}{2m} Im \int d\boldsymbol{v} \sum_\ell (\omega - \ell\Omega_c - k_\parallel v_\parallel)^{-1} \int d\boldsymbol{k}_\perp d\boldsymbol{k}'_\perp d\boldsymbol{q}_\perp \exp\left(i\ell[\varphi_k - \varphi_{k\prime}]\right) \\
&\quad \times \exp\left(i[\boldsymbol{k}_\perp - \boldsymbol{k}'_\perp] \cdot \boldsymbol{x}_\perp\right) \exp(i\boldsymbol{q}_\perp \cdot \boldsymbol{x}_\perp) J_0\left(\frac{v_\perp}{\Omega_c} |\boldsymbol{k}'_\perp - \boldsymbol{k}_\perp - \boldsymbol{q}_\perp|\right) \\
&\quad \times [\boldsymbol{C}_\ell(\boldsymbol{k}, \boldsymbol{q}_\perp, v_\perp, v_\parallel) \cdot \boldsymbol{E}(\boldsymbol{k}_\perp)] f_M(\boldsymbol{q}_\perp, v_\perp, v_\parallel) \left[\boldsymbol{B}_\ell(\boldsymbol{k}'_\perp, v_\perp, v_\parallel) \cdot \boldsymbol{E}(\boldsymbol{k}'_\perp)\right]^*,
\end{aligned} \tag{14}$$

$$\begin{aligned}
\boldsymbol{B}_\ell(\boldsymbol{k}_\perp, v_\perp, v_\parallel) &= v_\perp \left[\cos\varphi_k \frac{\ell}{\xi} J_\ell(\xi) - i \sin\varphi_k J'_\ell(\xi)\right] \boldsymbol{e}_x \\
&+ v_\perp \left[\sin\varphi_k \frac{\ell}{\xi} J_\ell(\xi) + i \cos\varphi_k J'_\ell(\xi)\right] \boldsymbol{e}_y \\
&+ v_\parallel J_\ell(\xi) \boldsymbol{e}_z, \\
\boldsymbol{C}_\ell(\boldsymbol{k}, \boldsymbol{q}_\perp, v_\perp, v_\parallel) &= \left[i\left(\frac{\boldsymbol{q}_\perp \cdot \boldsymbol{k}_\perp}{|\boldsymbol{k}_\perp|}\right) \frac{\ell}{\omega} J_\ell(\xi) + \frac{v_\perp}{\omega\Omega_c} (\boldsymbol{q}_\perp \times \boldsymbol{k}_\perp)_z J'_\ell(\xi)\right] (\sin\varphi_k \boldsymbol{e}_x - \cos\varphi_k \boldsymbol{e}_y) \\
&+ \frac{iv_\parallel}{\omega\Omega_c} J_\ell(\xi) (\boldsymbol{q}_\perp \times \boldsymbol{k}_\perp)_z \boldsymbol{e}_z + \frac{i}{\Omega_c} \left(\frac{k_\parallel v_\parallel}{\omega} - 1\right) J_\ell(\xi) (q_y \boldsymbol{e}_x - q_x \boldsymbol{e}_y).
\end{aligned} \tag{15}$$

In the homogeneous limit, $P^{(2)}$ vanishes and the local power becomes positive definite.

5 Larmor radius expansion

In many situations of a practical interest, the Larmor radius of the species ρ is small when compared to the characteristic scale length of the electric fields ($|\boldsymbol{k}|\rho \ll 1$) and the equilibrium quantities such as density and temperature ($|\boldsymbol{q}|\rho \ll 1$). The previously obtained expression (13) may then be expanded to any desired order to obtain a more explicit expression which can be handled by the computer.

Some rearrangements finally yield an expression for local power absorption in a

uniformly magnetized 2-D plasma, valid up to second order in the equilibrium and field gradients:

$$P_L(\boldsymbol{x}_\perp) = \sum_{\ell=-2}^{2} [P_\ell^{(1)} + P_\ell^{(2)}] \tag{16}$$

$$\begin{aligned}
P_{\ell=0}^{(1)} &= \frac{1}{8\pi}\left\{\rho^2\left(|(\boldsymbol{\nabla}\times\boldsymbol{E})_z|^2 + |(\boldsymbol{\nabla}\times\boldsymbol{E})_z - \frac{2\omega\Omega_c}{k_\parallel v_t^2}E_z|^2\right)\right. \\
&+ \left(\frac{\omega}{k_\parallel\Omega_c}\right)^2\left(\left|\frac{\partial E_z}{\partial x}\right|^2 + \left|\frac{\partial E_z}{\partial y}\right|^2 + 2Re(E_z^*\boldsymbol{\Delta}_\perp E_z)\right. \\
&\left.\left. + \frac{1}{2}|E_z|^2\boldsymbol{\Delta}_\perp + \left(\boldsymbol{\nabla}_\perp|E_z|^2\right)\cdot\boldsymbol{\nabla}_\perp\right)\right\}\tilde{Y}_0 \\
P_{\ell=\pm1}^{(1)} &= \frac{1}{8\pi}\left\{\frac{1}{2}\left|E_\pm + \frac{\Omega_{\pm1}}{k_\parallel\Omega_c}\left(\frac{\partial E_z}{\partial y} \mp i\frac{\partial E_z}{\partial x}\right)\right|^2\right. \\
&+ \left[\frac{1}{2}Re\left(\boldsymbol{E}_\perp{}^*\cdot[5\boldsymbol{\Delta}_\perp\boldsymbol{E}_\perp - 2\boldsymbol{\nabla}_\perp(\boldsymbol{\nabla}_\perp\cdot\boldsymbol{E})]\right.\right. \\
&\pm \left.\left. i\left(\boldsymbol{E}_\perp{}^*\times[5\boldsymbol{\Delta}_\perp\boldsymbol{E}_\perp - 2\boldsymbol{\nabla}_\perp(\boldsymbol{\nabla}_\perp\cdot\boldsymbol{E})]\right)_z\right)\right. \\
&\left.\left. + \left|\frac{\partial E_\pm}{\partial x}\right|^2 + \left|\frac{\partial E_\pm}{\partial y}\right|^2 + \frac{1}{2}|E_\pm|^2\boldsymbol{\Delta}_\perp + \left(\boldsymbol{\nabla}_\perp|E_\pm|^2\right)\cdot\boldsymbol{\nabla}_\perp\right]\rho^2\right\}\tilde{Y}_{\pm1} \\
P_{\ell=\pm2}^{(1)} &= \frac{1}{8\pi}\left\{\frac{\rho^2}{2}\left|\frac{\partial E_\pm}{\partial x} \pm i\frac{\partial E_\pm}{\partial y}\right|^2\right\}\tilde{Y}_{\pm2} \\
P_{\ell=0}^{(2)} &= \frac{1}{8\pi}Im\left\{(\boldsymbol{\nabla}\times\boldsymbol{E}^*)_z(\boldsymbol{E}\times\boldsymbol{\nabla})_z\frac{\omega_p^2 v_t^2}{2\omega\Omega_c^2}\right. \\
&\left. + E_z^*\left[(\boldsymbol{\nabla}_\perp E_z)\times\boldsymbol{\nabla}\right]_z\frac{i}{\omega\Omega_c}\left[\frac{\omega^2}{k_\parallel^2}\tilde{Z}_0 - \frac{\omega_p^2\omega}{k_\parallel^2}\right]\right\} \\
P_{\ell=\pm1}^{(2)} &= \frac{1}{8\pi}Im\left\{\pm E_\pm^*\left(\frac{\partial E_x}{\partial y} - \frac{\partial E_y}{\partial x}\right)\left(\frac{\partial}{\partial y} \mp i\frac{\partial}{\partial x}\right)\frac{v_t^2}{4\omega\Omega_c}\tilde{Z}_{\pm1}\right. \\
&\left. + E_\pm^*\left[\left[\left(\frac{\partial}{\partial x} \pm i\frac{\partial}{\partial y}\right)\boldsymbol{E}\right]\times\boldsymbol{\nabla}\right]_z\frac{iv_t^2}{4\Omega_c^2}\left(\frac{\Omega_c}{\omega}\tilde{Z}_{\pm1} \pm \frac{\omega_p^2}{\omega}\right)\right\} \\
P_{\ell=\pm2}^{(2)} &= 0
\end{aligned} \tag{17}$$

$$\begin{aligned}
E_\pm &= (E_x \pm iE_y), \quad \Omega_\ell = (\omega - \ell\Omega_c), \quad \rho = \left(\frac{T}{m\Omega_c^2}\right)^{1/2} \\
\tilde{Z}_\ell &= \frac{\omega_p^2}{(\omega-\ell\Omega_c)}Z_\ell^S, \quad Z_\ell = \frac{T}{m}\tilde{Z}_\ell, \qquad Z_\ell^S = Z^S\left(\frac{\omega-\ell\Omega_c}{|k_\parallel|v_t}\right)
\end{aligned} \tag{18}$$

where $Z^S = (X^S - iY^S)$ is the plasma dispersion function as defined by Shafranov (1967).

References

Gradshteyn I.S., Ryzhik I.M., *Table Of Integrals, Series And Products* (1965) Academic, New York

McVey B.D., Sund R.S., Scharer J.E. , *Phys. Rev. Lett.* **55** (1985) 507

Shafranov V.D. in *Reviews of Plasma Physics*, edited by M.A. Leontovich (Consultants Bureau, New York, 1967) Vol. **3**

Vaclavik J., Appert K., *Plasma Phys. and Contr. Fusion* **29** (1987) 257.

Yasseen F., Vaclavik J., *Phys. Fluids* **29** (1986) 450.

Analyses of Vlasov-Maxwell linear wave problems with large Larmor radii

O. Sauter and J. Vaclavik

Centre de Recherches en Physique des Plasmas
Association Euratom - Confédération Suisse
Ecole Polytechnique Fédérale de Lausanne
21, Av. des Bains, CH-1007 Lausanne - Switzerland

ABSTRACT

The linearized Vlasov-Maxwell equations for an inhomogeneous bounded slab plasma have been derived without any assumption on the ratio of the Larmor radius to the fluctuation wavelength and inhomogeneity scale. Only Maxwellian equilibrium distribution function, slowly varying magnetostatic field B_0 and $k_y = 0$ have been assumed. In this case, the equations consist of three second order integro-differential equations for each component of the elecric field. The first results of the code SEMAL, which solves these equations, are presented. They are compared with the results obtained with the code ISMENE, which solves these equations expanded to second order in the Larmor radii. Good agreement is found for the kinetic Alfvén wave and a small shift in frequency is found for the surface mode of the fast magnetosonic wave. A formula for the local power absorption is also derived, which consists of a positive-definite term, due to resonant particles absorption, and a non-resonant term which can be of either sign.

I. INTRODUCTION

The interaction of the waves and the plasma particles in the ion cyclotron range of frequencies (ICRF) is of main interest for better understanding the heating

mechanisms of tokamak plasmas. First cold and then warm models have been used to solve the linearized Vlasov-Maxwell equations expanded up to second order in the Larmor radii. These equations have been solved in 1-D and 2-D toroidal geometries.[1-3] These models are restricted by the condition that the product of the perpendicular wavenumber with the ion Larmor radius, $k_\perp \rho_i$, should be smaller than one. Therefore the models using an expansion in $k_\perp \rho_i$ are limited to wavelengths of at least one order of magnitude larger than ρ_i. This condition can easily be broken with the high temperatures reached in the tokamaks. The study of the interaction of heavier particles, like alpha particles, with the plasma or the interaction at higher harmonics also needs a model which does not use any assumption on the size of the parameter $k_\perp \rho_i$ or even $k_\perp \rho_e$. This model, called here hot model, has already been developed in the case of electrostatic waves interacting with an inhomogeneous bounded slab plasma.[4] In the present paper, we have extended the hot model to the electromagnetic waves, including the three components of the electric field. The physical model and the full integro-differential equations are presented in Sec.II. In Sec.III, we derive a formula for the local power absorption. Preliminary results of the code SEMAL are shown in Sec.IV, as well as a brief presentation of the numerical model, and we draw our conclusions in Sec.V.

II. PHYSICAL MODEL

The procedure is the same as for the electrostatic case, except that we have to use Maxwell's equations instead of Poisson's equation.[4] We start from the Vlasov equation, linearize it and take its Fourier transform. Then we solve for the perturbed distribution function $\tilde{f}^{(1)}(\mathbf{k}, \mathbf{v}, \omega)$ as a function of the equilibrium distribution function of the guiding centers and of the fields, which gives for isotropic temperature and plasma slab:[5]

$$\tilde{f}_\sigma^{(1)}(\mathbf{k},\mathbf{v},\omega) = \frac{i q_\sigma}{2\pi^{5/2} m_\sigma} e^{i\frac{(\mathbf{k}\wedge\mathbf{v})_z}{\omega_{c\sigma}}} \sum_n \frac{e^{-in\alpha}}{\omega - k_z v_z - n\omega_{c\sigma}} \int dx''\, dk'_x\, \frac{n_\sigma(x'')}{v_{T\sigma}^3(x'')}$$

$$e^{-\frac{v_\perp^2 + v_z^2}{v_{T\sigma}^2(x'')}} e^{-ik'_x x''} \left\{ P_x^n \left[\frac{2v_\perp}{v_{T\sigma}^2} \tilde{E}_x + i \frac{v_\perp k'_x}{\omega\, \omega_{c\sigma}} ((k_x - k'_x)\tilde{E}_y - k_y \tilde{E}_x) \right] \right. \quad (1)$$

$$\left. + P_y^n \frac{2v_\perp}{v_{T\sigma}^2} \tilde{E}_y + \mathfrak{J}_n \left[\frac{2v_z}{v_{T\sigma}^2} \tilde{E}_z - i(\omega - k_z v_z) \frac{k'_x \tilde{E}_y}{\omega\, \omega_{c\sigma}} - i \frac{k_y k'_x v_z \tilde{E}_z}{\omega\, \omega_{c\sigma}} \right] \right\},$$

with

$$\mathbf{v} = (v_\perp, \alpha, v_z),$$

$$\tilde{E}_\nu = \tilde{E}_\nu (k_x - k'_x, k_y, k_z, \omega),$$

$$P_\nu^n = P_\nu^n (k_x - k'_x, k_y, k_z, \omega),$$

$$P_x^n(\mathbf{k}_\perp) = \frac{1}{2}[\mathfrak{J}_{n+1}(\mathbf{k}_\perp) + \mathfrak{J}_{n-1}(\mathbf{k}_\perp)],$$

$$P_y^n(\mathbf{k}_\perp) = \frac{i}{2}[\mathfrak{J}_{n-1}(\mathbf{k}_\perp) - \mathfrak{J}_{n+1}(\mathbf{k}_\perp)],$$

$$\mathfrak{J}_n(\mathbf{k}_\perp) = J_n\left(\frac{|\mathbf{k}_\perp| v_\perp}{\omega_{c\sigma}}\right) e^{in\varphi}, \quad \tan\varphi = \frac{k_y}{k_x},$$

and where q_σ, m_σ, $v^2_{T\sigma} = 2T_\sigma/m_\sigma$ and $\omega_{c\sigma}$ are the charge, mass, thermal velocity and cyclotron frequency of species σ, respectively. n_σ and T_σ are the density and temperature of the guiding centers. J_n is the Bessel function and the magnetostatic field B_0 is parallel to the z direction.

Closure equation is obtained through combination of Maxwell's equations and the relation between the current density and the perturbed distribution function :

$$\mathbf{j}(\mathbf{r}, \mathbf{v}, t) = \sum_\sigma q_\sigma \int \mathbf{v} f_\sigma^{(1)}(\mathbf{r}, \mathbf{v}, t)\, d^3\mathbf{v}$$

Taking Fourier transform, the closure equation is the following:

$$\mathbf{k}\wedge\mathbf{k}\wedge\tilde{\mathbf{E}} + \frac{\omega^2}{c^2}\tilde{\mathbf{E}} + \sum_{\sigma} i\mu_0\omega q_\sigma \int \mathbf{v}\,\tilde{f}_\sigma^{(1)}(\mathbf{k},\mathbf{v},\omega)\,d^3\mathbf{v} = 0, \tag{2}$$

Substituting Eq.1 into Eq.2, introducing a Maxwellian equilibrium distribution function, and integrating over velocity, we obtain:

$$\mathbf{k}\wedge\mathbf{k}\wedge\tilde{\mathbf{E}} + \frac{\omega^2}{c^2}\tilde{\mathbf{E}} + i\mu_0\omega\,\underline{\tilde{\sigma}}\,\tilde{\mathbf{E}} = 0, \tag{3}$$

with

$$\underline{\tilde{\sigma}}\,\tilde{\mathbf{E}} \equiv \sum_{\sigma,n} -\frac{i q_\sigma^2}{2\pi m_\sigma k_z}\int dx''\,dk'_x\,\frac{n_\sigma(x'')}{v_{T\sigma}(x'')}\,e^{-i(k_x-k'_x)x''}\,e^{-\frac{1}{2}(k_\perp^2+k'^2_x)\rho_\sigma^2}\,\underline{\hat{\sigma}}(k'_x)\,\tilde{\mathbf{E}}(k'_x),$$

and

$$\hat{\sigma}_{xx}(k'_x) = \frac{(n\omega_{c\sigma})^2}{k_\perp k'_x}\,Z_n\,I_n\left(\frac{2}{v_{T\sigma}^2} - i\frac{k_y(k_x-k'_x)}{\omega\,\omega_{c\sigma}}\right),$$

$$\hat{\sigma}_{yy}(k'_x) = Z_n\,\rho_\sigma^2\left[k_\perp k'_x I_n - (k_\perp^2 + k'^2_x - \rho_\sigma^{-2})I'_n + k_\perp k'_x I''_n\right] - \frac{k_z v_{T\sigma}}{\omega}\,(k'_x - k_\perp)^2\,\rho_\sigma^2\,I_n,$$

$$\hat{\sigma}_{zz}(k'_x) = v_{T\sigma}^2\,\xi_n(1+\xi_n Z_n)\,I_n\left(\frac{2}{v_{T\sigma}^2} - i\frac{k_y(k_x-k'_x)}{\omega\,\omega_{c\sigma}}\right),$$

$$\hat{\sigma}_{xy}(k'_x) = i\frac{n}{k_\perp}\,Z_n\,(k_\perp I'_n - k'_x I_n),$$

$$\hat{\sigma}_{yx}(k'_x) = -i\frac{n v_{T\sigma}^2}{2k'_x}\,Z_n\,(k'_x I'_n - k_\perp I_n)\left(\frac{2}{v_{T\sigma}^2} - i\frac{k_y(k_x-k'_x)}{\omega\,\omega_{c\sigma}}\right),$$

$$\hat{\sigma}_{xz}(k'_x) = \frac{n\omega_{c\sigma}v_{T\sigma}}{k_\perp}\,(1+\xi_n Z_n)\,I_n\left(\frac{2}{v_{T\sigma}^2} - i\frac{k_y(k_x-k'_x)}{\omega\,\omega_{c\sigma}}\right),$$

$$\hat{\sigma}_{zx}(k'_x) = \frac{n\omega_{c\sigma}v_{T\sigma}}{k'_x}\,(1+\xi_n Z_n)\,I_n\left(\frac{2}{v_{T\sigma}^2} - i\frac{k_y(k_x-k'_x)}{\omega\,\omega_{c\sigma}}\right),$$

$$\hat{\sigma}_{yz}(k'_x) = -i\frac{v_{T\sigma}^3}{2\omega_{c\sigma}}(1+\xi_n Z_n)(k'_x I'_n - k_\perp I_n)\left(\frac{2}{v_{T\sigma}^2} - i\frac{k_y(k_x-k'_x)}{\omega\,\omega_{c\sigma}}\right),$$

$$\hat{\sigma}_{zy}(k'_x) = i\frac{v_{T\sigma}}{\omega_{c\sigma}}(1+\xi_n Z_n)(k_\perp I'_n - k'_x I_n),$$

$$I_n = I_n(k_\perp k'_x \rho_\sigma^2) \quad , \quad Z_n = Z(\xi_n) \quad , \quad \xi_n = \frac{\omega - n\omega_{c\sigma}}{|k_z| v_{T\sigma}},$$

where I_n is the modified Bessel function, Z is the Fried-Conte plasma dispersion function, and $\rho^2_\sigma = v^2_{T\sigma}/2\omega^2_{c\sigma}$ is the Larmor radius. In the case of homogeneous profile, both integrals in Eq.3 disappear and we recover the standard dispersion relation for electromagnetic waves.[6]

At this point, we shall assume $k_y = 0$ in $\tilde{\sigma}$, neglecting k_y versus k_x in the dielectric response of the plasma. Moreover, as typically $k_y\rho_i << 1$, we are entitled to use this approximation as long as we do not consider drift waves. In order to take the inverse Fourier transform of Eq.3, we use the same integral representation for I_n as in the electrostatic case:[4]

$$I_n(z) = \frac{1}{\pi}\int_0^\pi e^{z\cos\theta}\cos(n\theta)\,d\theta \quad . \tag{4}$$

Introducing Eq.4 into Eq.3 and integrating over k_x and k'_x, we obtain the three integro-differential equations:

$$\nabla\wedge\nabla\wedge\mathbf{E}(x) - \frac{\omega^2}{c^2}\mathbf{E}(x) - i\mu_0\omega(\underline{\underline{\sigma}}\mathbf{E})(x) = 0, \tag{5}$$

with

$$(\underline{\sigma}\,\mathbf{E})(x) \equiv \sum_{\sigma,\,n} -\frac{i q_\sigma^2}{2\pi m_\sigma k_z} \int dx''\, dx' \int_0^\pi d\theta\, \frac{n_\sigma(x'')}{v_{T\sigma}(x'')}$$

$$\exp\left\{-\frac{(x-x'')^2 - 2(x-x'')(x'-x'')\cos\theta + (x'-x'')^2}{2\rho_\sigma^2(x'')\sin^2\theta}\right\}\ \bar{\underline{\sigma}}(x,x',x'',\theta)\,\mathbf{E}(x')$$

$$\bar{\sigma}_{xx} = -\frac{n Z_n}{\pi\rho_\sigma^2}\sin n\theta\,,$$

$$\bar{\sigma}_{yy} = -\frac{Z_n}{\pi\rho_\sigma^4}(x-x'')(x'-x'')\frac{\cos n\theta}{\sin\theta} - \frac{\sqrt{2\pi}k_z v_{T\sigma}}{\omega\rho_\sigma}\left(\frac{(x-x'')^2}{\rho_\sigma^2} - 1\right) e^{\frac{(x-x'')^2}{2\rho_\sigma^2}}\,\delta(x-x')\,\delta(\theta-\frac{\pi}{2})\,,$$

$$\bar{\sigma}_{zz} = -\frac{2}{\pi\rho_\sigma^2}\xi_n(1+\xi_n Z_n)\frac{\cos n\theta}{\sin\theta}\,,$$

$$\bar{\sigma}_{xy} = \frac{iZ_n}{\pi\rho_\sigma^4}(x'-x'')\left[(x-x'')\cos\theta - (x'-x'')\right]\frac{\sin n\theta}{\sin^2\theta}\,,$$

$$\bar{\sigma}_{yx} = -\frac{iZ_n}{\pi\rho_\sigma^4}(x-x'')\left[(x'-x'')\cos\theta - (x-x'')\right]\frac{\sin n\theta}{\sin^2\theta}\,,$$

$$\bar{\sigma}_{xz} = -\frac{2i\omega_{c\sigma}}{\pi\rho_\sigma^2 v_{T\sigma}}\xi_n Z_n\left[(x-x'')\cos\theta - (x'-x'')\right]\frac{\sin n\theta}{\sin^2\theta}\,,$$

$$\bar{\sigma}_{zx} = \frac{2i\omega_{c\sigma}}{\pi\rho_\sigma^2 v_{T\sigma}}\xi_n Z_n\left[(x'-x'')\cos\theta - (x-x'')\right]\frac{\sin n\theta}{\sin^2\theta}\,,$$

$$\bar{\sigma}_{yz} = \frac{2\omega_{c\sigma}}{\pi\rho_\sigma^2 v_{T\sigma}}(1+\xi_n Z_n)(x-x'')\frac{\cos n\theta}{\sin\theta}\,,$$

$$\bar{\sigma}_{zy} = \frac{2\omega_{c\sigma}}{\pi\rho_\sigma^2 v_{T\sigma}}(1+\xi_n Z_n)(x'-x'')\frac{\cos n\theta}{\sin\theta}\,.$$

These equations are valid to all orders in ion and electron Larmor radii, for any density and temperature profiles of the guiding centers and for weakly inhomogeneous magnetic field. It applies mainly to the ICRF and the Alfvén wave range of frequencies, but not to drift wave problems. The restriction to $k_y=0$ in $\underline{\sigma}$ imposes a lower bound to the frequency range, but Eq.5 still holds for very high

frequencies.

The singular points of the theta integral, at $\theta=\pm\pi$, can be removed by using the same changes of variables as for the electrostatic case.[4]

III. LOCAL POWER ABSORPTION

Following the steps of Ref.7, we are able to define a local power absorption formula where the energy flux due to particles streaming into and out the volume element is not taken into account:

$$P_L(x) = \mathrm{Re}\sum_\sigma \frac{q_\sigma}{2}\int d^3v\, dk_\perp\, dk''_\perp\, \tilde{\mathbf{E}}^*(\mathbf{k}''_\perp)\left\langle \mathbf{v}'\, \tilde{f}_\sigma^{(1)}(\mathbf{k}_\perp,\mathbf{v}')\, e^{i(\mathbf{k}_\perp-\mathbf{k}''_\perp)\mathbf{x}'_\perp}\right\rangle_t , \qquad (6)$$

where $<..>_t$ denotes the time-average and $\mathbf{x}',\mathbf{v}'$ are the Lagrangian coordinates representing the position and velocity of a particle moving along an unperturbed orbite.[7] Then, we introduce Eq.1 into Eq.6 and integrate over k_x and k''_x by means of the same integral representation of the Bessel function J_n as in Ref.4. We obtain, with $k_y=0$, a formula for the local power absorption of the wave in an inhomogeneous bounded plasma valid to all orders in the Larmor radii:

$$P_L(x) = \sum_{n,\sigma}\frac{2q_\sigma^2}{\pi^{5/2}m_\sigma|k_z|}\int dx''\int_0^{\frac{\pi}{2}} d\theta\, \frac{n_\sigma(x'')\,\omega_{c\sigma}^4(x'')}{v_{T\sigma}^5(x'')}\exp\left\{-\frac{(x-x'')^2}{2\rho_\sigma^2\cos^2\theta}\right\}\frac{|x-x''|}{\cos^2\theta}$$

$$e^{-\xi_{n\sigma}^2(x'')}\left|\int dx'\left[iE_x(x')\sin n\bar{u} - \frac{\cos\bar{u}\cos n\bar{u}}{\sin\bar{u}}\left(E_y(x') - \frac{\omega-n\omega_{c\sigma}}{k_z(x'-x'')\omega_{c\sigma}}E_z(x')\right)\right]\right|^2 \qquad (7)$$

$$+\sum_\sigma\int dx''d\theta\,\frac{n_\sigma(x'')q_\sigma^2\omega_{c\sigma}^2(x'')}{\pi^2 m_\sigma v_{T\sigma}^2(x'')\omega\cos\theta}\exp\left\{-\frac{(x-x'')^2}{2\rho_\sigma^2\cos^2\theta}\right\}\int dx'\,\frac{(x''-x')}{\sin\bar{u}}\,\mathrm{Im}[E'_y(x')E_y^*(x')] .$$

with

$$\bar{u}(x') = \arccos\left(\frac{x'' - x'}{|x'' - x|}\cos\theta\right) \quad , \quad \sin\bar{u} \geq 0 \, ,$$

and where the x' interval of integration is such that $-1 < \cos\bar{u} < 1$. The first term, corresponding to the contribution of the resonant particles, is positive-definite, whereas the second term, which is a non resonant term, may be of either sign. It is difficult to compare the amplitude of these terms, but we do not expect any instabilities with $k_y=0$. We have not found cases where the second term is non negligible, except very close to the boundary where a very sharp drop occurs due to some kind of electromagnetic Debye screening, as discussed in next section. Eq.7 recovers the positive-definite formula of Ref.4 if we introduce the electrostatic potential approximation. In this approximation, with $k_y=0$, E_y vanishes and the second term disappears.

IV. RESULTS

In this paper, we shall show only preliminary results of the code SEMAL, which solves Eq.5. The numerical method used in SEMAL is the same as in the code SEAL, which solves the electrostatic approximation of Eq.5.[4] Thus, we use the finite element method and we integrate analytically over x" and x', after having replaced the x" integral by a sum of integrals over homogeneous short intervals. In this paper, we shall consider only homogeneous profiles, therefore one interval for x" is sufficient. Besides, Eq.5 consists of two second order, for E_y and E_z, and one first order, for E_x, integro-differential equations. In consequence, we take linear basis functions for E_y, E_z and piece-wise constant for E_x, in order to avoid pollution problems due to the $(\nabla\wedge\nabla\wedge)$ operator.[8] As we shall compare SEMAL with the code ISMENE,[9] which solves Eq.5 expanded to second order in Larmor radii, we use the same boundary conditions. That is, the plasma is surrounded by vacuum, which is itself limited by perfectly conducting walls. The antenna is localized in the vacuum at the right-hand side of the plasma. The current in the antenna flows parallel to the

y direction. The parameters used are the following: $n_e=n_i=10^{19}$ m^{-3}, $T_e=1000$ eV, $T_i=10$ eV, $B_0=1$ T, $x_{sr}=-x_{sl}=12$ cm, $x_{pr}=-x_{pl}=8$ cm, $x_{ant}=8.8$ cm, $k_y=5$ m^{-1}, $k_z=3$ m^{-1}, deuterium plasma. We compare the power emitted by the antenna in the Alfvén wave range of frequencies, that is for $\omega/\omega_{ci}=0.25$ up to 0.75, as seen in Fig.1. The value of $k_z c_A/\omega_{ci}$ is 0.3 for these parameters, where $c_A^2=B_0^2/\mu_0 nm$ is the Alfvén velocity. The peaks of the kinetic Alfvén wave (KAW) and of the surface mode of the fast magnetosonic wave can be seen from SEMAL (dashed line), and from ISMENE (solid line). The first two modes of the KAW can be detected and they appear at the same frequencies for the two codes. For the first mode of the KAW, we show in Fig.2 and 3 the imaginary part of E_x, which is the dominant component. As in the electrostatic case,[4] there is a sharp drop at the edge which scales with the Debye length of the electrons and which is mainly electrostatic (Fig.3b).

The peak of the surface mode has a slight shift in frequency between the two codes. This is not surprising as, on the one hand, the dispersion relation is represented differently in the two codes. On the other hand, the condition at the plasma-vacuum interface is very different. Indeed, in ISMENE, there is a sharp drop of the density of the particles, whereas in SEMAL, the density of the guiding centers is discontinuous, but not the density of particles. This difference has a strong influence at both sides of the trace in Fig.1, where the power obtained from ISMENE (solid line) becomes negative. This is why we have used, at the lower part of Fig.1, a "negative logarithmic" scale. The dotted points illustrate that the line would be continuous with a linear scaling. This non-physical feature is due to the discontinuity mentioned above and is removed in the code SEMAL (dashed line).

The local absorption power density $P_L(x)$ for $\omega/\omega_{ci}=0.445$, corresponding to the surface mode, is shown in Fig.4a. In this case, the contribution due to the non resonant term is three orders of magnitude smaller than the one due to the

positive-definite term. Here, only the electron Cerenkov resonance contributes to the local power absorption. Fig.4b shows the local power integrated over x from the right-hand side of the plasma. We see that the sharp drops at the edges do not contribute to the total power absorbed in the plasma.

V. CONCLUSION

We have derived the linearized Vlasov-Maxwell equations for an inhomogeneous bounded slab plasma valid to all orders in the Larmor radii. Only Maxwellian equilibrium distribution function, $k_y=0$, and weakly inhomogeneous magnetic field have been assumed. The equations are two second order integro-differential equations for E_y and E_z, and one first order integro-differential equation for E_x.

We also derived a formula for the local power absorption of the field. This formula consists of a positive-definite term, due to resonant particles, and another smaller term, due to non resonant particles, which may be of either sign.

A code, SEMAL, solving these integro-differential equations and computing the local power absorption has been developed. It solves these equations for a slab plasma surrounded by vacuum and limited by perfectly conducting walls. The

the Debye screening observed in the electrostatic case.[4] This drop shows up mainly in the E_x component. We have shown, however, that this drop does not contribute to the power absorbed in the plasma.

ACKNOWLEDGEMENTS

The authors wish to thank Dr. K. Appert for useful discussions and for providing us the numerical code ISMENE.

This work was partly supported by the Swiss National Science Foundation.

REFERENCES

1 A. Fukuyama, K. Itoh, and S.-I. Itoh, Comput. Phys. Rep. 4, 137 (1986).

2 D. Edery and H. Picq, Comput. Phys. Commun. 40, 95 (1986).

3 M. Brambilla and T. Krücken, Nucl. Fusion 28, 1813 (1988).

4 O. Sauter, J. Vaclavik, and F. Skiff, Phys. Fluids B 2, 475 (1990).

5 F. Yasseen and J. Vaclavik, Phys. Fluids 29, 450 (1986).

6 A. B. Mikhailovskii, in Reviews of Plasma Physics, edited by A. M. Leontovich (Consultants Bureau, New York, 1966), Vol.3, p. 166.

7 J. Vaclavik and K. Appert, Plasma Phys. Controlled Fusion 29, 257 (1987).

8 X. Llobet, K. Appert, A. Bondeson, and J. Vaclavik, Comput. Phys. Commun. 59, 199 (1990).

9 K. Appert, T. Hellsten, H. Lütjens, O. Sauter, J. Vaclavik, and L. Villard, in Proceedings of the International Conference on Plasma Physics, Kiev, Invited Papers, edited by A.G. Sitenko (World Scientific, Singapore, 1987), p. 1230.

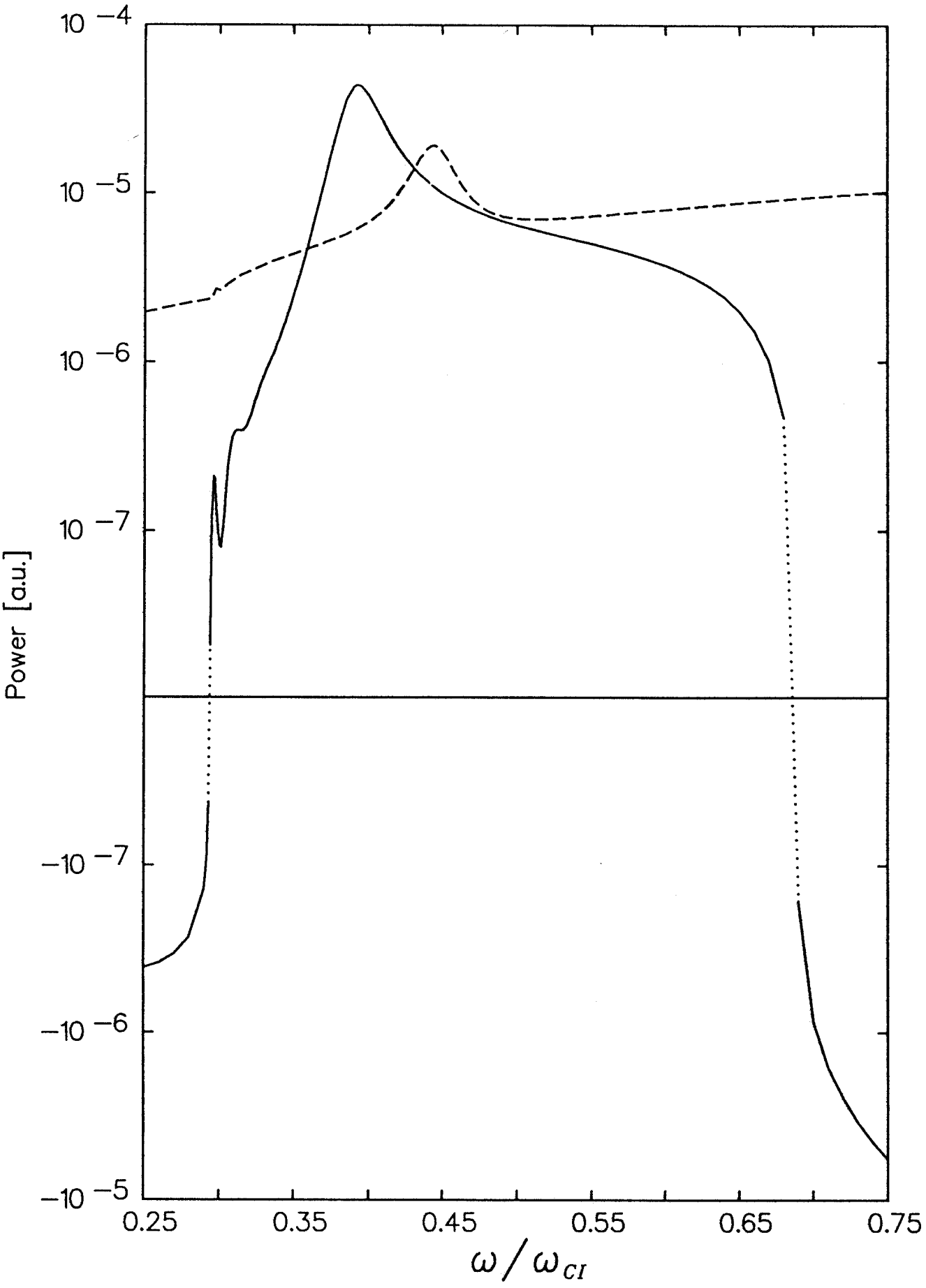

FIG.1. Power emitted by antenna vs. ω/ω_{ci} from ISMENE (solid line) and SEMAL (dashed line). The small peaks around $\omega/\omega_{ci}=0.3$ are due to KAW, whereas the large broad peak is due to the surface mode of the fast wave. The power is negative for $\omega/\omega_{ci}<0.293$ and $\omega/\omega_{ci}>0.69$ for ISMENE, therefore a "negative logarithmic" scale has been used for the lower part of the plot.

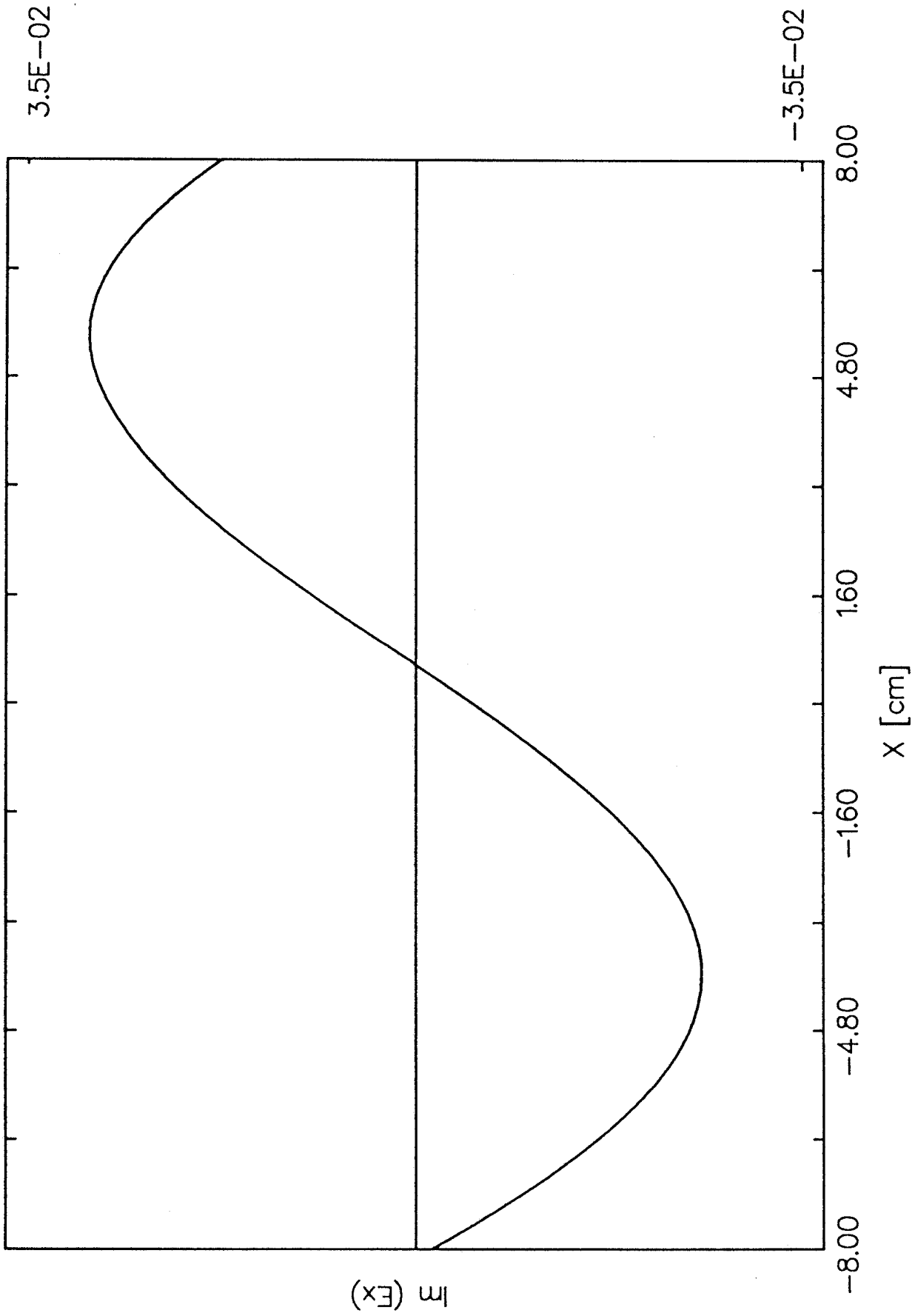

FIG.2. Imaginary part of E_x obtained with ISMENE for the first mode of the KAW, at ω/ω_{ci}=0.296.

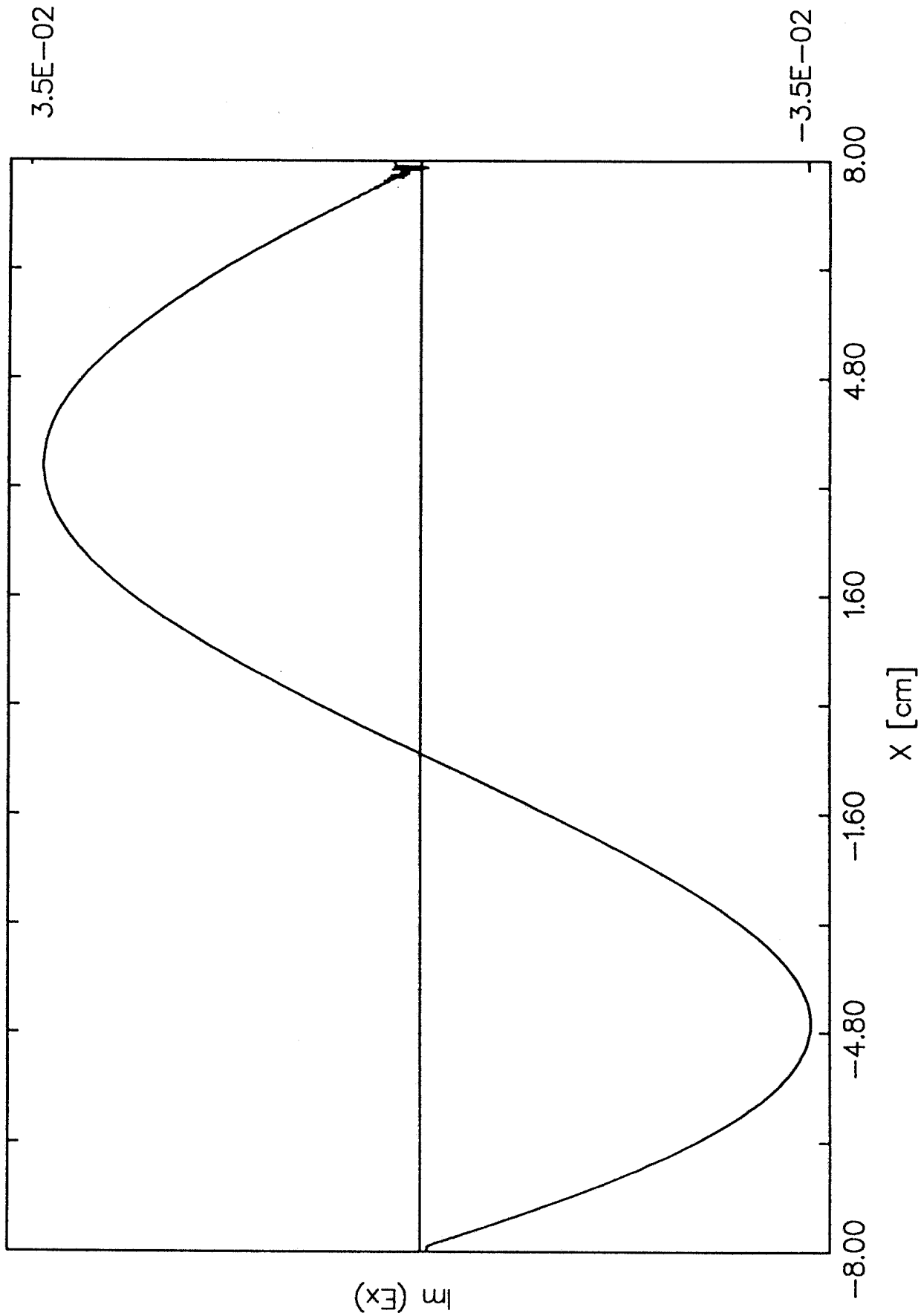

FIG.3a. Imaginary part of E_x obtained with SEMAL for the first mode of the KAW, at ω/ω_{ci}=0.298. The same scale has been used as in Fig.2. The edge parts of the field have been cut at ± 7.94 cm. They are shown in Fig.3b.

FIG.3b. Edge parts of $Im(E_x)$ shown in Fig.3a. The same units have been used. The mesh points are represented by the dots, showing that this fine structure is resolved numerically.

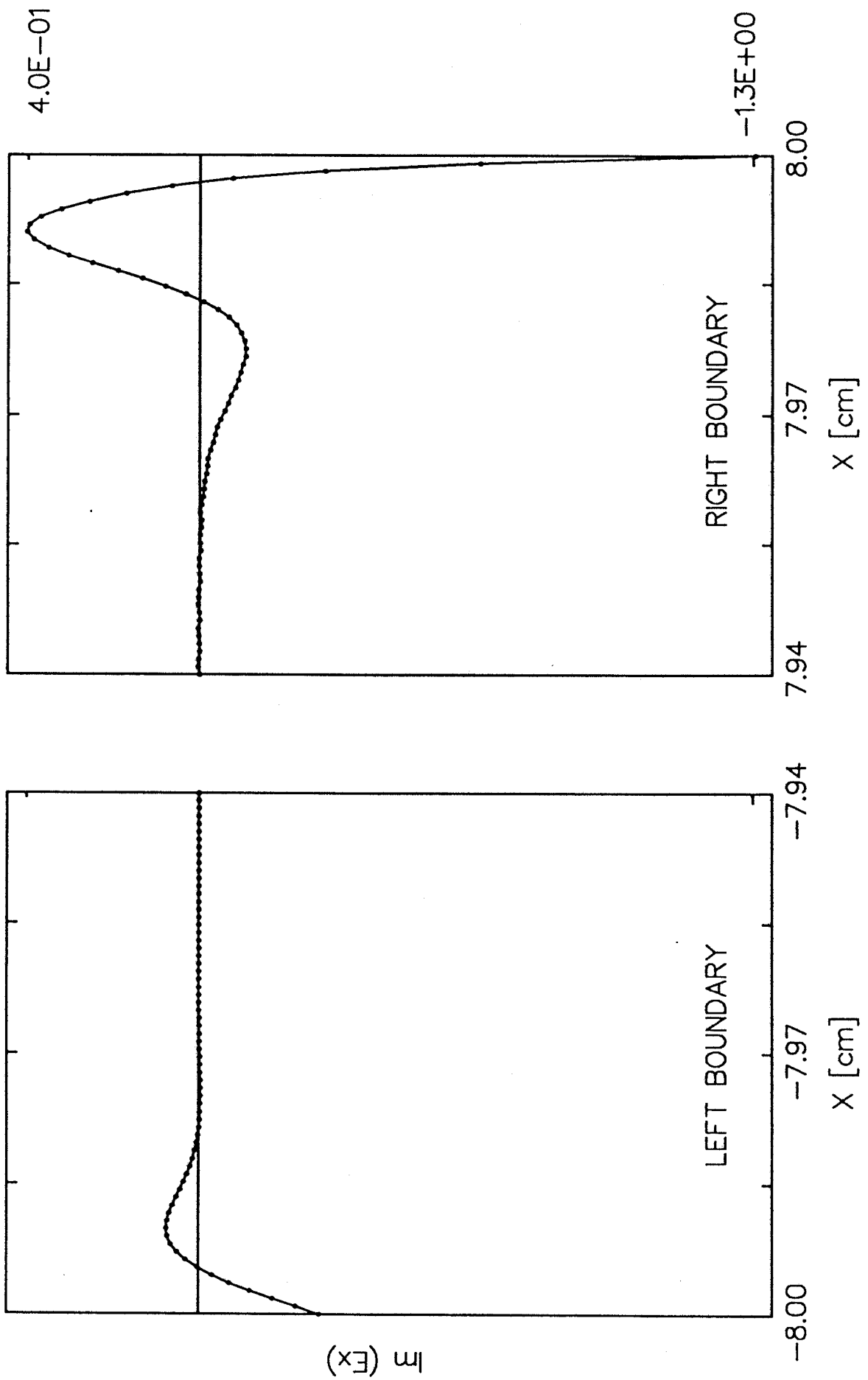

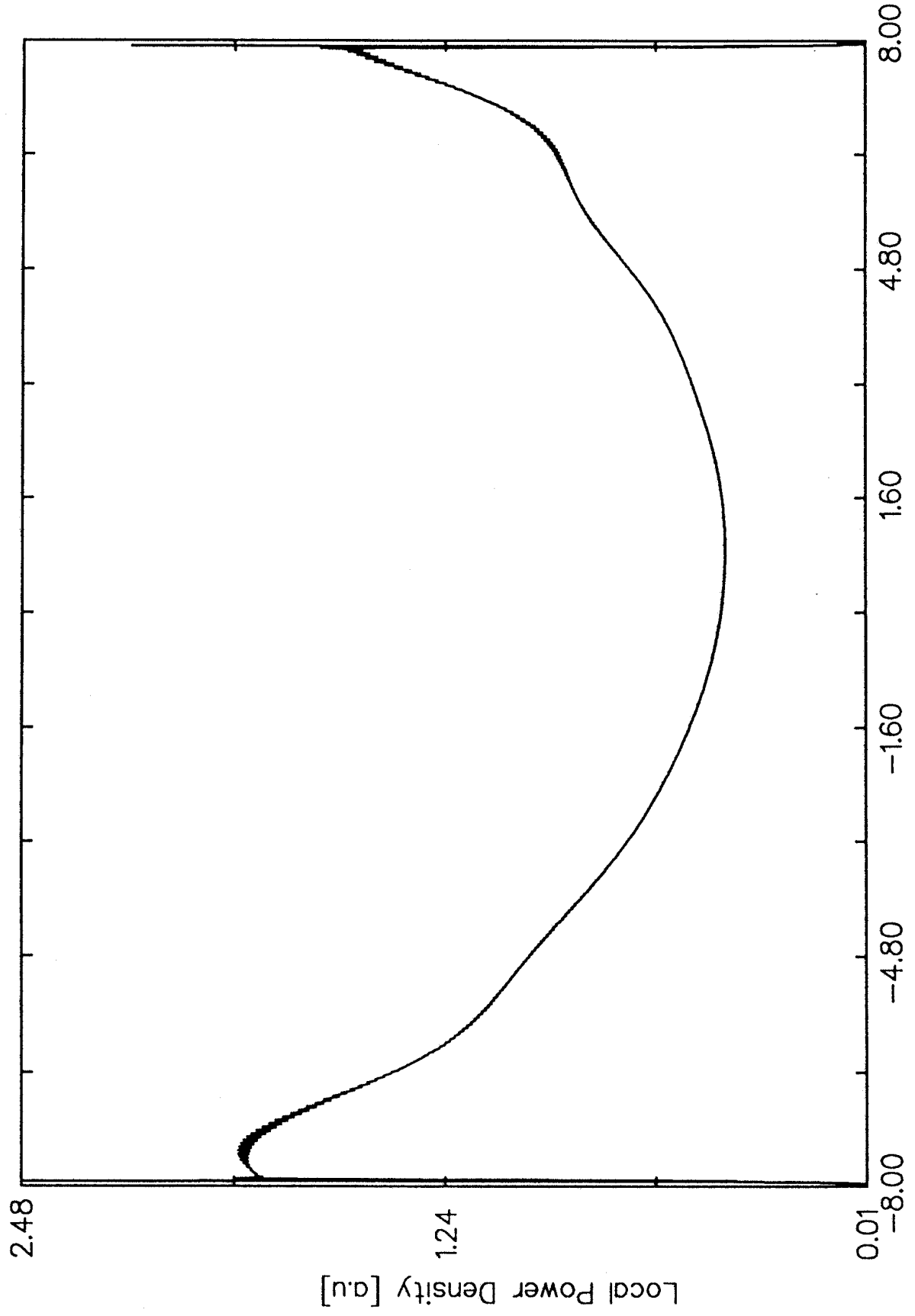

FIG.4a. Local power density $P_L(x)$ obtained from SEMAL at ω/ω_{ci}=0.445, that is at the peak due to the surface mode.

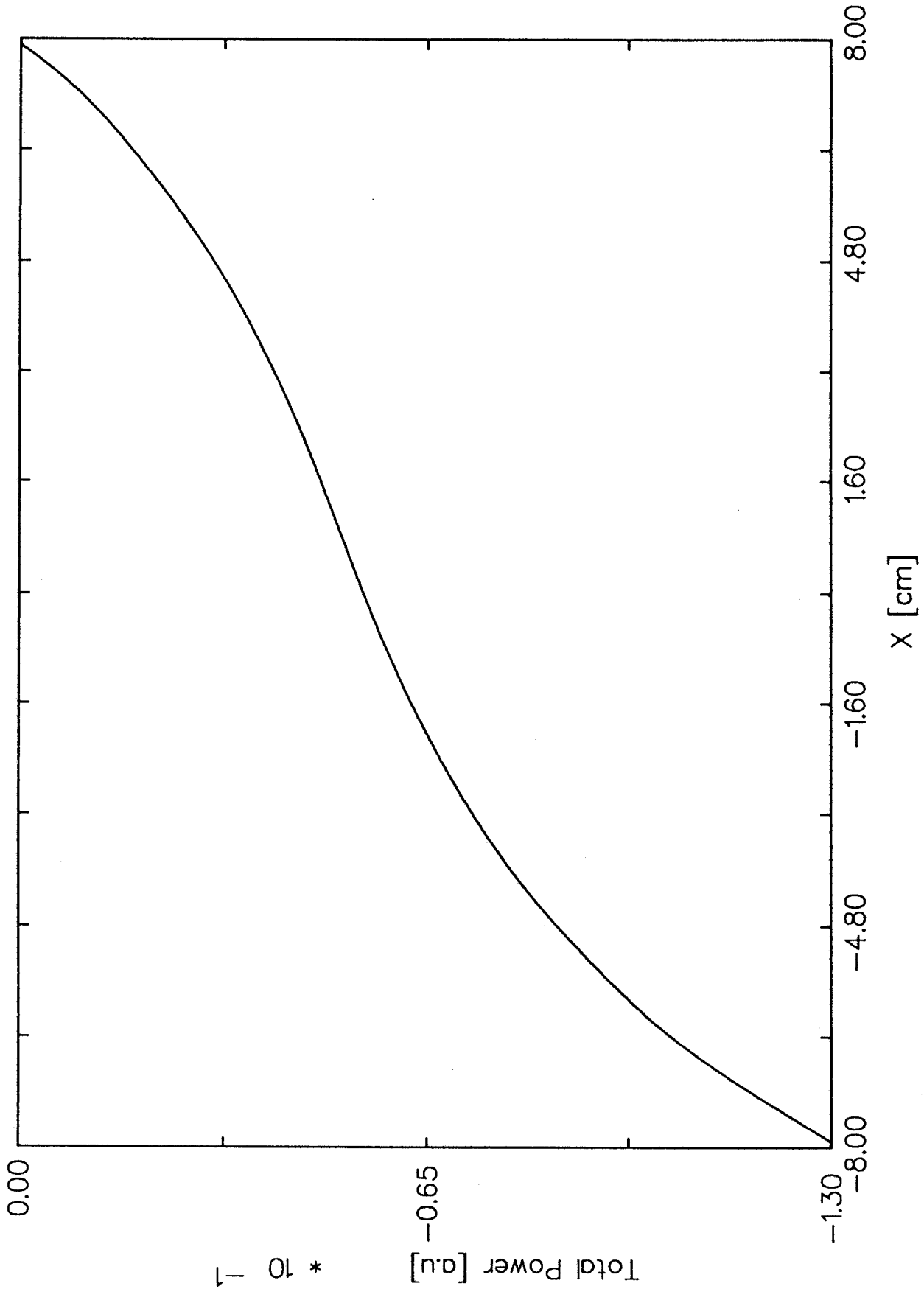

FIG.4b. Total power absorbed in plasma, obtained by integrating $P_L(x)$, shown in Fig.4a, from the right-hand side of the plasma.